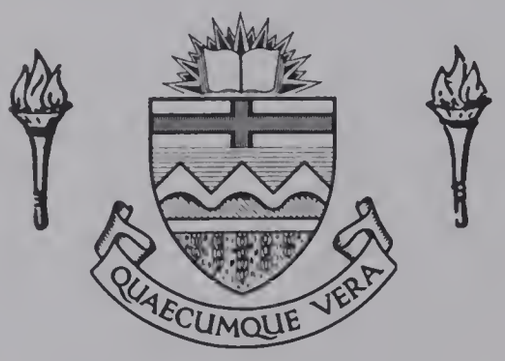

THE UNIVERSITY OF ALBERTA

INVESTIGATION OF A DIAPHRAGM TYPE LOAD CELL

by

AMIT KUMAR SAHA, B.M.E. (JADAVPUR)

A THESIS

SUBMITTED TO THE FACULTY OF GRADUATE STUDIES

IN PARTIAL FULFILMENT OF THE REQUIREMENTS FOR THE DEGREE

OF MASTER OF SCIENCE

DEPARTMENT OF MECHANICAL ENGINEERING

EDMONTON, ALBERTA

APRIL, 1968

UNIVERSITY OF ALBERTA

FACULTY OF GRADUATE STUDIES

The undersigned certify that they have read, and recommend to the Faculty of Graduate Studies for acceptance, a thesis entitled "Investigation of a Diaphragm Type Load Cell" submitted by AMIT KUMAR SAHA in partial fulfilment of the requirements for the degree of Master of Science.

ABSTRACT

A diaphragm type load cell having a stepped-up central region is theoretically analyzed and experimental results are compared with the theory. The diaphragm is optimized on the basis of the theoretical results and a procedure is set up to design a diaphragm type load transducer for a particular load range. A comparison of the diaphragm type load cell with two other commonly employed transducer elements, the cylindrical type and the fork type, is presented. This comparison has been made on the basis of the same overall size for load range, sensitivity and frequency response.

ACKNOWLEDGEMENTS

The author expresses his sincerest thanks to the following:

-- Dr. D. G. Bellow without whose supervision and guidance the thesis could not have been presented in this form,
-- The staff members of the Mechanical Engineering Department, especially, Messrs. Arnold, Smart, Simpson, and Marak, for extending their best help in the experimental work,
-- The friends and colleagues of the department, for their suggestions and encouragement,
-- Miss Gertrude Dole for the excellent typing of the thesis,
-- Du Pont of Canada Limited and the National Research Council for the financial support of the research through scholarship and NRC Grants A4762 (Kennedy) and A2705 (Bellow).

TABLE OF CONTENTS

LIST OF SYMBOLS

a - outer radius of diaphragm

b - radius of stepped-up portion of diaphragm, radius of uniformly loaded area in case of diaphragm of uniform thickness

d - diameter of the cylindrical element,

- depth of the load bearing cross-section of the fork element

D - plate rigidity

D_h - plate rigidity for thickness h

D_H - plate rigidity for thickness H

e - strain

e_c - sum of two strains

e_r - radial strain

e_t - tangential strain

$\bar{e}_t$ - average tangential strain

E - Young's modulus of elasticity

f - frequency of natural vibration of transducer

g - gravitational constant

h - thickness of the diaphragm at the thinner portion

H - thickness of the diaphragm at the thicker portion

ℓ - length of the cylindrical element

- distance between the load application point and the center of the load bearing cross-section of the fork element

M_r - radial moment per unit length

M_t - tangential moment per unit length

P - total load

q - uniform pressure

Q_r - shear force per unit length

r - radius

t - depth of tine of the fork element

w - deflection

  - width of the fork element

α - ratio of plate rigidities D_H to D_h

γ - specific weight of material

σ_l - allowable stress in material

σ_r - radial stress

σ_t - tangential stress

σ_x - stress in x-direction

η - sensitivity

LIST OF TABLES

LIST OF FIGURES

CHAPTER I

INTRODUCTION

1.1 History

The design of transducers for measuring pressures and loads has received the attention of scientists and engineers for a considerable time. The development of strain gauges in the late 1930's made it possible to design transducers with more accuracy and dependability. Grey[1]* has given a comparative evaluation of a strain gauge as an element of a pressure transducer and other similar elements like capacitance, crystal and reluctance types. In the late 1940's and early 1950's Bierman and Jenkins,[2] and Bierman[3] successfully employed the diaphragm type transducers with strain gauges as physical and hypodermic pressure manometers. Wenk[4] devised a diaphragm type transducer to measure low pressures in fluids, and Werner[5] developed a systematic procedure for designing a diaphragm for measuring pressure in 1953. Hitherto, a diaphragm was used to measure pressure only.

In 1966, Lee,[6] on behalf of the Center for Highway Research, University of Texas, employed a diaphragm, illustrated in Figure 1, as a "Load Transducer" in a "portable" scale for weighing vehicles in motion. As a result of this application the Research Council of Alberta, Highways Division, experimented on diaphragms of the same shape and made of hardened tool steel (Atlas Keewatin Steel). Unfortunately, a few of the load cells cracked in the load range of 8000 to 9000 pounds. This suggested a theoretical and experimental investigation of the stresses and deflections of the diaphragm for different geometrical parameters.

*Superscripts denote the reference number in the Bibliography.

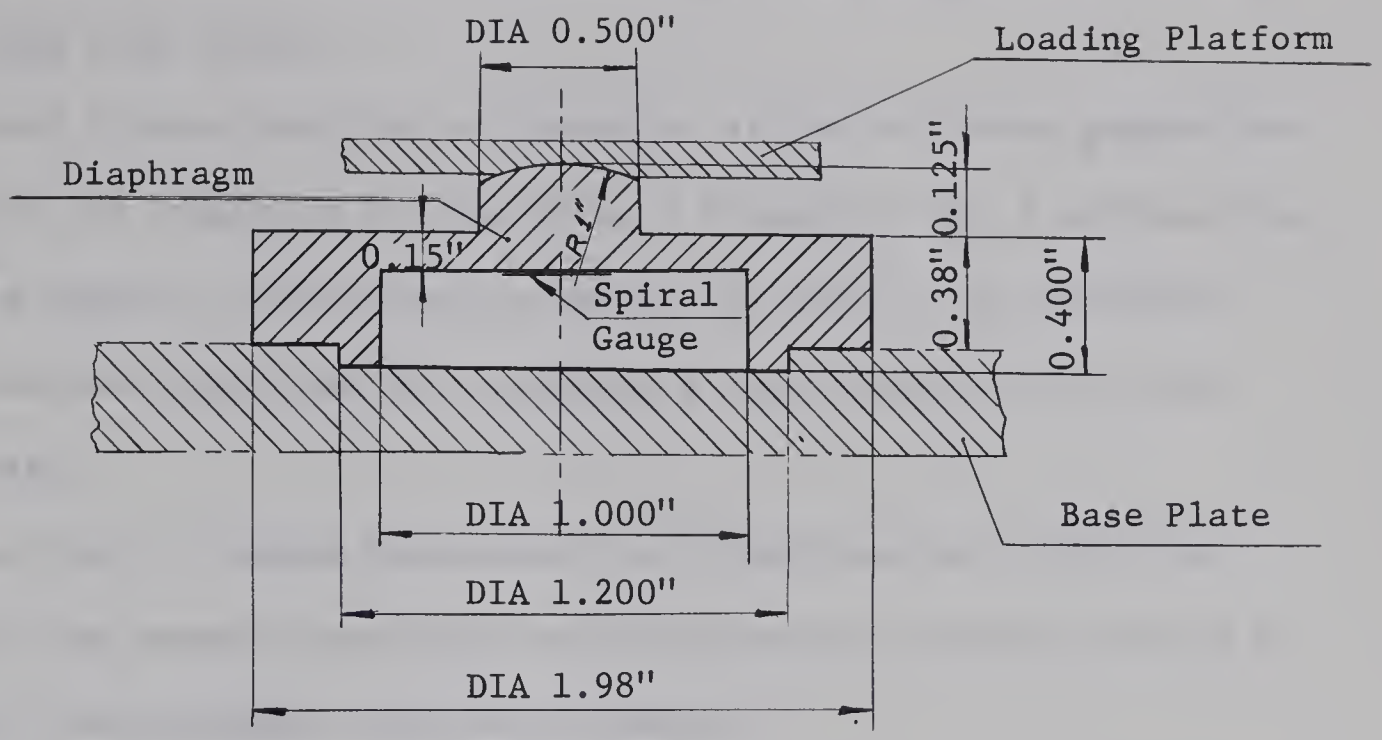

FIGURE 1. Load Cell or Diaphragm

1.2 Aim of Thesis

The aims of this thesis are; first, to analyze the diaphragm type force transducer for stresses and deflections in relation to the geometrical parameters and the applied force; secondly, to optimize the geometrical parameters of the diaphragm for a maximum load range and set up a systematic procedure for designing an optimum load transducer; and finally, to compare the diaphragm type load transducer with some of the commonly employed load transducers.

1.3 Plan of Thesis

In Part A, a theoretical analysis of the problem has been sought by different methods after necessary idealizations have been made for the nature of loading and the shape of the diaphragm. These theoretical

results have been compared with those obtained from experiments on two diaphragm type load cells.

Part B deals with the optimization of the different geometrical parameters of the diaphragm for designing a transducer for a maximum load range on the basis of the analysis presented in Part A. A systematic procedure has been laid down for designing a load transducer with the optimized data.

In Part C, design procedures for cylindrical and fork type transducers, two commonly employed load transducers, have been set up to compare with the diaphragm type load transducer.

PART A

DIAPHRAGM TYPE LOAD TRANSDUCER

CHAPTER II

THEORETICAL ANALYSIS

2.1 General

An attempt is made in this chapter to theoretically analyze the stresses and deflections of the diaphragm, shown in Figure 1, by idealizing the shape of the diaphragm and the nature of the load distribution. The theories and methods which may be applied to this idealized diaphragm are

i) the theory of three dimensional elasticity for bodies bounded by a surface of revolution,

ii) a simplified method by treating the central thick portion as a rigid body acting as a load distributor,

iii) the thin plate theory,

iv) the generalized plane stress theory or moderately thick plate theory as suggested by Love.[7]

In this work, solutions have been obtained by the last three methods and steps have been suggested to obtain a solution by the first method.

2.2 Idealization of Shape and the Loading Shape:

The diaphragm of Figure 1 has been idealized to the shape shown in Figure 2 by eliminating the radius at the top of the boss and the projection at the bottom. It is assumed that this simplification will not affect the stresses and strains in the zone of interest of the diaphragm.

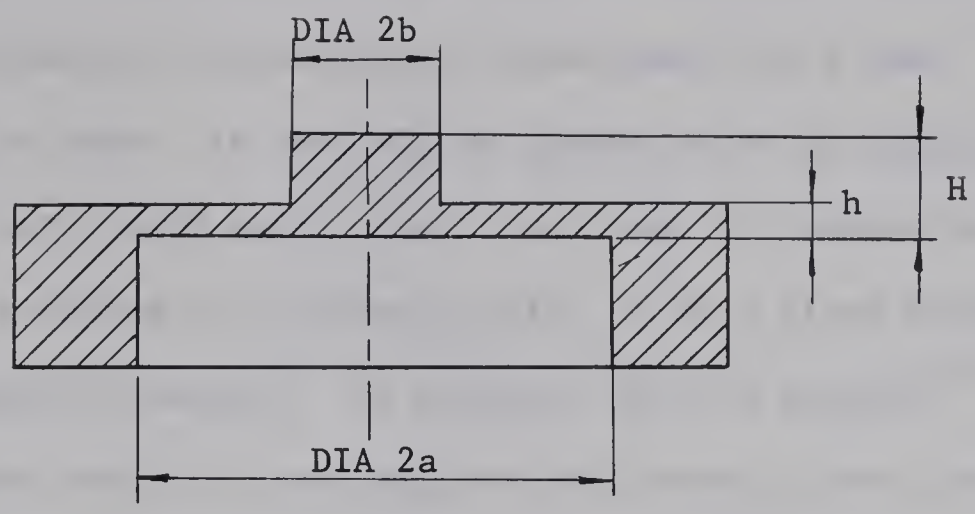

FIGURE 2. Idealized Diaphragm

Loading:

In the load transducer, Figure 1, used by the Center for Highway Research, University of Texas, the load was transmitted by the top plate through the mating surfaces to the top of the boss of the diaphragm. Because of the nature of surface contact, it is difficult to predict the actual distribution of load intensity over the boss. For analysis the load may be assumed to be concentrated at the center, but the disadvantages of this assumption are as follows;

i) Under the load application point, the radial stresses due to bending moments by both the thin plate theory and the generalized plane stress theory suggested by Love[7] become infinite.

ii) Under the load application point, the stress normal to the surface of the boss and the shear stress due to the concentrated load become infinite. The thin plate theory and Love's moderately thick plate theory do not take into account the effect of the normal stress and shear stress; and hence, are unsuitable for this particular case.

iii) In practice, a concentrated load cannot be achieved because of local yielding and the subsequent development of a load distribution area. It can only be approximated by applying the load over a very small area, e.g., area of contact of two spherical surfaces of different radii, or of a plane surface with a spherical surface. By applying Hertz's formula[8] it may be shown that the resulting stresses even at very low loads, for such surfaces in contact, are large enough to cause yielding. Yielding, in turn, causes a change in the area of contact and in the load distribution, making the problem difficult to investigate.

Because of the disadvantages of applying a concentrated load, it is proposed to distribute the load uniformly over the boss area in order to analyze the problem theoretically and check it experimentally.

Edge Condition:

The edge of the diaphragm in Figure 2 is not clamped in the strict sense of the word, though it approaches the clamped edge condition with the use of a heavier rim at radius $r = a$. Hence, for theoretical analysis the boundary condition is taken as clamped edge condition.

2.3 Three-Dimensional Approach

The diaphragm of Figure 2 may be considered to consist of two parts as shown in Figure 3. The top part, treated as a solid body bounded by a surface of revolution, is in equilibrium under the action of a uniform external pressure of q on the top surface, and the reactive shear force Q and moment M per unit length along the circumference $2\pi b$ over the height h.

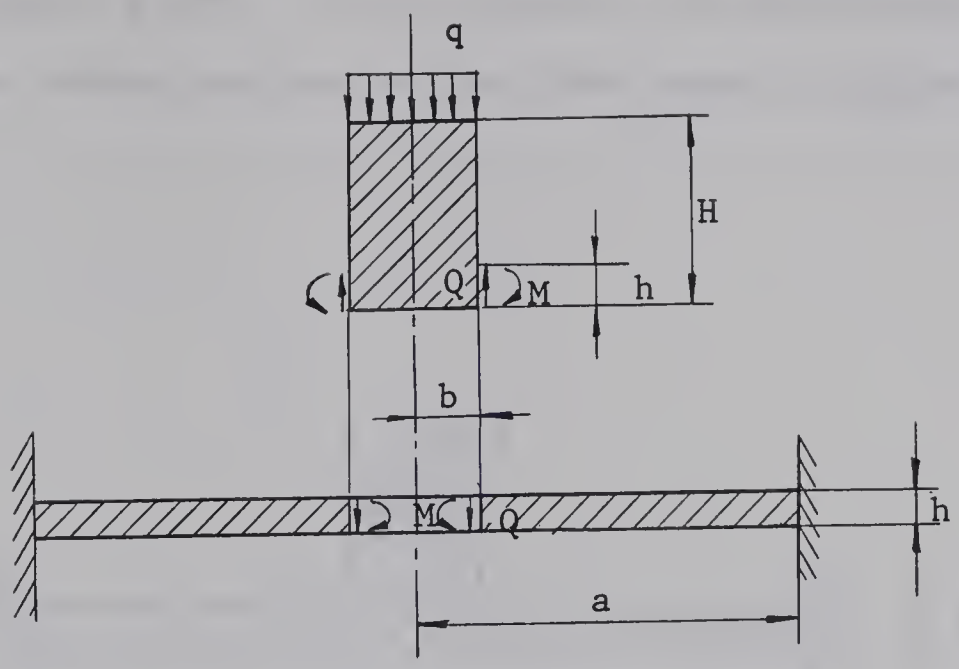

FIGURE 3. Clamped Edge Diaphragm

The solution is to be obtained from the theory of three dimensional elasticity as indicated by Timoshenko.[9] The other part may be treated as a circular annular plate clamped at the outer edge and acted on by a radial moment M and a shear force Q per unit length along the inner boundary. The magnitudes of M and Q are such that the deflection, slope, and strain at radius $r = b$ must be the same for both the parts. Obtaining such a solution is extremely difficult because of the fact that the shear force and the moment are applied over only a part of the cylindrical body and a polynomial of very high degree is required for solving such a problem.

Without using the three dimensional approach, a simplified method has been adopted to obtain the solution to the problem in the next section.

2.4 Simplified Method

In this method, it is assumed that the highly stepped-up central

portion acting as a rigid body, without being deformed itself, distributes the load to the annular plate. On this premise, the plate shown in Figure 4(b) is analyzed to obtain results for the plate shown in Figure 4(a).

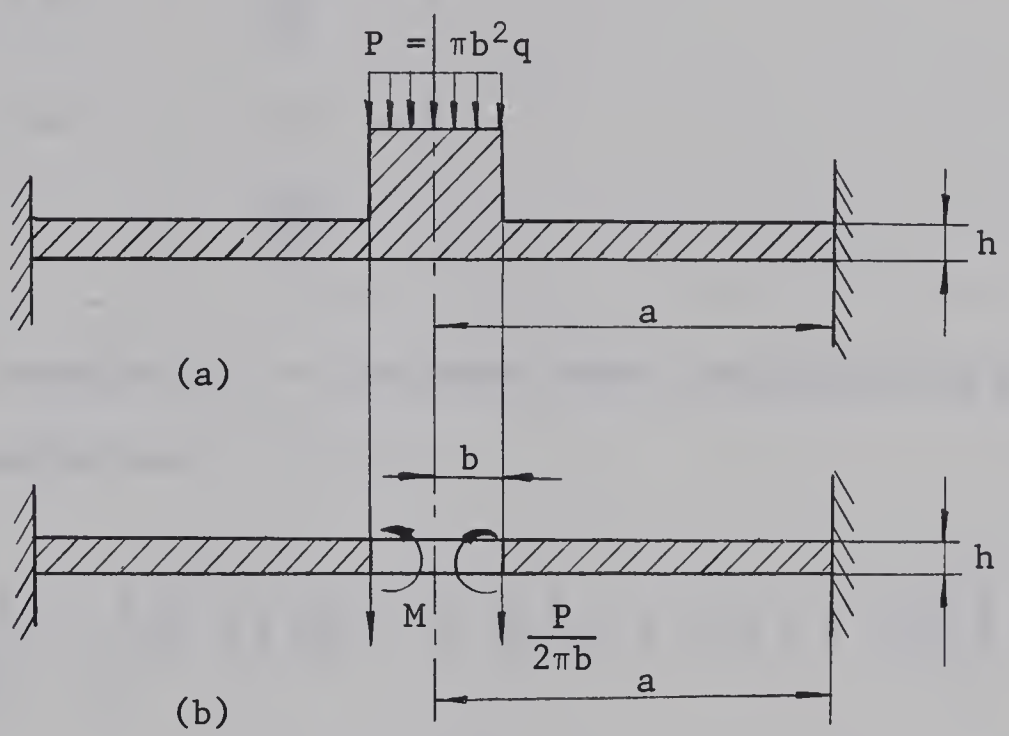

FIGURE 4. Diaphragm

Because of the rigidity of the central portion, the slope at radius $r = b$ is zero. The loading on the plate, Figure 4(b), is equivalent to a shearing force $\frac{P}{2\pi b}$ per unit length along the inner boundary at radius $r = b$. The governing differential equation for this axi-symmetrical plate is

$$\frac{d}{dr}\left[\frac{1}{r}\frac{d}{dr}\left(r\frac{dw}{dr}\right)\right] = \frac{P}{2\pi bD} \quad .$$

The solution to this equation is

$$w = \frac{Pr^2}{8\pi D}\left[\ln\frac{r}{a} - 1\right] + C_1\frac{r^2}{4} + C_2\ln\frac{r}{a} + C_3 \; ; \quad \text{for } b \leqslant r \leqslant a,$$

where C_1, C_2, C_3 are the integration constants to be determined from the following boundary conditions:

$$\text{at} \quad r = b, \qquad \frac{dw}{dr} = 0$$

$$\text{at} \quad r = a, \qquad w = 0$$

$$\frac{dw}{dr} = 0 \; .$$

Substituting the equation for w in these three conditions and solving for constants, the results are

$$w = \frac{Pa^2}{16\pi D}\frac{1}{\left(\frac{a^2}{b^2} - 1\right)}\left[\frac{r^2}{a^2}\left\{2\left(\frac{a^2}{b^2} - 1\right)\ln\frac{r}{a} + 2\ln\frac{b}{a} + 1 - \frac{a^2}{b^2}\right\}\right.$$

$$\left. - 4\ln\frac{b}{a}\ln\frac{r}{a} + \frac{a^2}{b^2} - 1 - 2\ln\frac{b}{a}\right] \quad \ldots \text{ for } b \leqslant r \leqslant a$$

$$\ldots (1)$$

$$M_r = \frac{P(1+\mu)}{8\pi}\frac{1}{\left(\frac{a^2}{b^2} - 1\right)}\left[\left(1 - \frac{a^2}{b^2}\right)\left(2\ln\frac{r}{a} + \frac{1-\mu}{1+\mu}\right) - 2\ln\frac{b}{a} + 1 - \frac{a^2}{b^2}\right.$$

$$\left. - 2\,\frac{1-\mu}{1+\mu}\,\frac{a^2}{r^2}\ln\frac{b}{a}\right] \quad \ldots \text{ for } b \leqslant r \leqslant a$$

$$\ldots (2)$$

$$\sigma_r = \frac{6}{h^2}M_r \qquad \ldots (2a)$$

where M_r is given by equation (2).

Since the central region is assumed infinitely stiff, this solution does not tell anything about the stresses and deflections in the zone $0 \leqslant r \leqslant b$ of Figure 4(a). Radial moment M_r from equation (2) has been plotted for various $\frac{b}{a}$ ratios in Figures 9 and 10. Deflection w for various $\frac{b}{a}$ ratios has been shown in Figures 7 and 8 using equation (1).

2.5 Thin Plate Theory

The cross-section shown in Figure 2 is idealized to the shape shown in Figure 5, and then the thin plate theory is used to derive the deflections and the stresses of the diaphragm. Hoeland[10] used this type of idealization in analyzing a stepped rectangular plate, but he did not present any experimental verification.

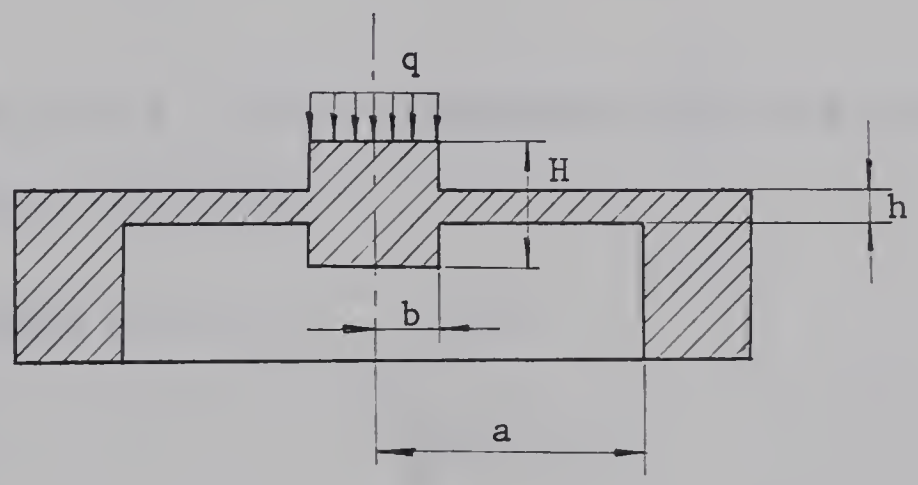

FIGURE 5. Symmetrically Stepped-Up Diaphragm

In thin plate theory, deflection w satisfies the following biharmonic equations:

$$\nabla^4 w_1 = \frac{q}{D_H} \quad ; \qquad 0 \leqslant r \leqslant b \ , \qquad \ldots (3)$$

$$\nabla^4 w_2 = 0 \quad ; \qquad b \leqslant r \leqslant a \ , \qquad \ldots (4)$$

where for the axi-symmetrical case in polar co-ordinates

$$\nabla^4 = \left(\frac{d^2}{dr^2} + \frac{1}{r}\frac{d}{dr}\right)\left(\frac{d^2}{dr^2} + \frac{1}{r}\frac{d}{dr}\right) \ .$$

The solutions of equations (3) and (4) are given by the following equations:

$$w_1 = \frac{qr^4}{64D_H} + A_1 + B_1 r^2 \quad ; \qquad 0 \leqslant r \leqslant b \ , \qquad (5)$$

$$w_2 = A_2 + B_2 r^2 + C_2 \ln\frac{r}{a} + D_2 r^2 \ln\frac{r}{a} \quad ; \quad b \leqslant r \leqslant a, \qquad \ldots (6)$$

where A_1, B_1, A_2, B_2, C_2, D_2 are the integration constants to be evaluated from the following conditions;

Boundary Conditions at $r = a$, $\quad w_2 = 0$

$$\frac{dw_2}{dr} = 0 \ ,$$

Continuity equations at $r = b$, $\quad w_1 = w_2$

$$\frac{dw_1}{dr} = \frac{dw_2}{dr}$$

$$M_{r1} = M_{r2}$$

$$Q_{r1} = Q_{r2} \ .$$

Radial moment M_r and shear force Q_r are given by the following equations:

$$M_r = -D \left[\frac{d^2w}{dr^2} + \frac{\mu}{r}\frac{dw}{dr}\right]$$

$$Q_r = -D \left[\frac{d^3w}{dr^3} + \frac{1}{r}\frac{d^2w}{dr^2} - \frac{1}{r^2}\frac{dw}{dr}\right] .$$

On solving the constants by using the conditional equations, the final results are

$$w_1 = \frac{qb^4}{64D_H}\left[\left(\frac{r}{b}\right)^4 + \left\{1 + 4\alpha\left(\frac{a^2}{b^2} - 1\right) + 8\frac{a^2}{b^2}\alpha\, N \ln\frac{b}{a}\right\}\right.$$

$$\left. + 2\frac{r^2}{b^2}\left\{2\alpha\, N\left(\frac{a^2}{b^2} - 1\right) + 4\alpha \ln\frac{b}{a} - 1\right\}\right] \quad ; \quad 0 \leq r \leq b, \qquad \ldots (7)$$

$$w_2 = \frac{qa^2b^2\alpha}{16D_H}\left[(1 + N)\left(1 - \frac{r^2}{a^2}\right) + 2 \ln\frac{r}{a}\left\{N + \frac{r^2}{a^2}\right\}\right] \quad ; \quad b \leq r \leq a, \qquad \ldots (8)$$

$$M_{r1} = -\frac{qb^2}{16}\left[\frac{r^2}{b^2}(3 + \mu) + (1 + \mu)\left\{2\alpha\, N\left(\frac{a^2}{b^2} - 1\right) + 4\alpha\, N \ln\frac{b}{a} - 1\right\}\right];$$

$$0 \leq r \leq b, \qquad \ldots (9)$$

$$M_{r2} = -\frac{qb^2}{16}\left[-2(1 + \mu)(1 + N) - 2\left(\frac{a}{r}\right)^2 N(1 - \mu) + 4(1 + \mu) \ln\frac{r}{a} + 2(3 + \mu)\right];$$

$$b \leq r \leq a, \qquad \ldots (10)$$

$$M_{t1} = -\frac{qb^2}{16}\left[\frac{r^2}{b^2}\,(1+3\mu) + (1+\mu)\left\{2\alpha\, N\,(\frac{a^2}{b^2}-1) + 4\alpha\, \ln\frac{b}{a} - 1\right\}\right];$$

$$0 \leqslant r \leqslant b, \qquad \ldots (11)$$

$$M_{t2} = -\frac{qb^2}{16}\left[-2(1+\mu)\,(1+N) + 2(1-\mu)N\,\frac{a^2}{r^2} + 4(1+\mu)\,\ln\frac{r}{a} + 2(1+3\mu)\right];$$

$$b \leqslant r \leqslant a, \qquad \ldots (12)$$

where $N = \dfrac{1}{1+\mu}\;\dfrac{1 + 2(1+\mu)\,(1-\alpha)\,\ln\frac{b}{a}}{(\frac{a^2}{b^2}-1)\alpha + 1 + \frac{a^2}{b^2}\,\frac{1-\mu}{1+\mu}}$.

$$\sigma_{r1} = \frac{6}{H^2}\,M_{r1} \qquad \ldots (9a)$$

$$\sigma_{r2} = \frac{6}{h^2}\,M_{r2} \qquad \ldots (10a)$$

$$\sigma_{t1} = \frac{6}{H^2}\,M_{t1} \qquad \ldots (11a)$$

$$\sigma_{t2} = \frac{6}{h^2}\,M_{t2} \qquad \ldots (12a)$$

where M_{r1}, M_{r2}, M_{t1} and M_{t2} are given by equations (9) to (12).

Deflection w and radial moment M_r computed from equations (7) to (10) for various $\frac{H}{h}$ and $\frac{b}{a}$ ratios are shown in Figures 7 to 10.

2.6 Generalized Plane Stress Theory or Moderately Thick Plate Theory

Love suggested using a generalized plane stress theory to solve plate problems where the thickness to radius ratio is greater than 0.1. The assumptions for a generalized plane stress system are

i) σ_z, the stress normal to the plane of plate (X-Y plane), as shown in Figure 6, is zero throughout the thickness,

ii) σ_{zx} and σ_{zy} are zero on the plate surfaces $z = 0$ and $z = h$, but do not vanish inside.

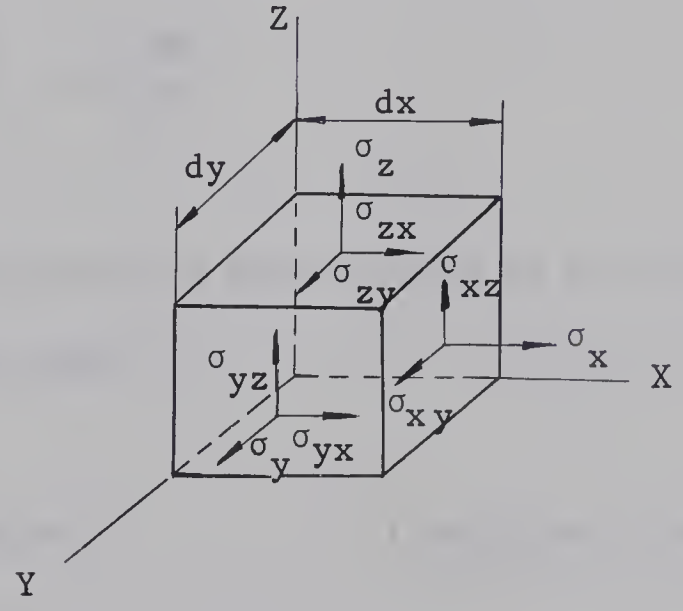

FIGURE 6. Plate Element

The basic differential equations and their solutions are the same as equations (3), (4), (5) and (6) for the case discussed using thin plate theory. The boundary conditions and the continuity equations also remain the same as given in the thin plate theory. Love presents the following equations for moments in the middle plane of the plate on the basis of

related stress functions:

$$M_{r1}^{(11)} = -D_H\,(\bar{k}_1 + \mu\bar{k}_2) - \frac{8 + \mu + \mu^2}{80\,(1 - \mu)}\,qH^2 \;; \quad 0 \leqslant r \leqslant b \qquad \ldots (13)$$

$$M_{r2}^{(12)} = -D_h\,\nabla^2 w_2 + D_h\,(1 - \mu)\,\frac{1}{r}\frac{d}{dr}\left(w_2 + \frac{1}{40}\,\frac{8 + \mu}{1 - \mu}\,h^2\nabla^2 w_2\right) ;$$

$$b \leqslant r \leqslant a \qquad \ldots (14)$$

where for axi-symmetrical cases in plane polar co-ordinates

$$\nabla^2 = \frac{d^2}{dr^2} + \frac{1}{r}\frac{d}{dr}$$

$$\bar{k}_1 = \frac{d^2 w_1}{dr^2}$$

$$\bar{k}_2 = \frac{1}{r}\frac{dw_1}{dr} \;.$$

Love's notations have been changed in the following manner to conform to the present work:

Love's notation	Notation in this work
$2H$	H
$2h$	h
$\frac{1}{\rho'}\ \frac{\partial}{\partial\nu}$	$\frac{1}{r}\frac{d}{dr}$
p	$-q$

Using equations (13) and (14) for M_r, the final results are

$$w_1 = \frac{qa^4}{16D_h}\left[\frac{1}{4\alpha}\left(\frac{r}{a}\right)^4 - \left(\frac{b}{a}\right)^4 \overline{A}_1 - \frac{b^2}{a^2}\cdot\frac{r^2}{a^2}\cdot\overline{B}_1\right]; \quad 0 \leqslant r \leqslant b \qquad \ldots (15)$$

$$w_2 = \frac{qa^4}{16D_h}\left[\frac{b^2}{a^2}\left(1 - \frac{b^2}{a^2}N\right)\left(1 - \frac{r^2}{a^2}\right) - 2\frac{b^2}{a^2}\left(N\frac{b^2}{a^2} - \frac{r^2}{a^2}\right)\ln\frac{r}{a}\right];$$

$$b \leqslant r \leqslant a \qquad \ldots (16)$$

$$M_{r1} = \frac{qb^2}{16}\left[-\frac{r^2}{b^2}(3+\mu) + 2(1+\mu)\alpha\,\overline{B}_1 - \frac{8+\mu+\mu^2}{5(1-\mu)}\frac{H^2}{b^2}\right];$$

$$0 \leqslant r \leqslant b \qquad \ldots (17)$$

$$M_{r2} = \frac{qb^2}{16}\left[2(1+\mu)\left(1 - \frac{b^2}{a^2}N\right) - 2(1-\mu)\frac{b^2}{r^2}N - 2(3+\mu)\right.$$

$$\left. - 4(1+\mu)\ln\frac{r}{a} + \frac{8+\mu}{5}\frac{h^2}{r^2}\right]; \quad b \leqslant r \leqslant a \qquad \ldots (18)$$

$$M_{t1} = \frac{qb^2}{16}\left[-\frac{r^2}{b^2}(1+3\mu) + 2(1+\mu)\alpha\,\overline{B}_1 - \frac{8+\mu+\mu^2}{5(1-\mu)}\frac{H^2}{b^2}\right];$$

$$0 \leqslant r \leqslant b \qquad \ldots (19)$$

$$M_{t2} = \frac{qb^2}{16}\left[2(1+\mu)\left(1 - \frac{b^2}{a^2}N\right) + 2\frac{b^2}{r^2}(1-\mu)N - 4(1+\mu)\ln\frac{r}{a}\right.$$

$$\left. - 2(1+3\mu) - \frac{8+\mu}{5}\frac{h^2}{r^2}\right]; \qquad b \leqslant r \leqslant a \qquad \ldots (20)$$

where $$N = \frac{2(\alpha - 1)\ \ln \frac{b}{a} + \frac{1}{10} \cdot \frac{8 + \mu}{1 + \mu} \frac{h^2}{b^2} + \frac{1}{10} \frac{8 + \mu + \mu^2}{1 - \mu^2} \frac{H^2}{b^2} - \frac{1}{1 + \mu}}{\alpha + \frac{1 - \mu}{1 + \mu} - \frac{b^2}{a^2} (\alpha - 1)}$$

$$\overline{A}_1 = 1 - \frac{a^2}{b^2} + 2N \ln \frac{b}{a} - \frac{1}{4\alpha}$$

$$\overline{B}_1 = N \left(1 - \frac{b^2}{a^2}\right) - 2 \ln \frac{b}{a} + \frac{1}{2\alpha} \cdot$$

$$\sigma_{r1} = \frac{6}{H^2} M_{r1} \ ; \qquad 0 \leqslant r \leqslant b, \qquad \ldots (17a)$$

$$\sigma_{r2} = \frac{6}{h^2} M_{r2} \ ; \qquad b \leqslant r \leqslant a, \qquad \ldots (18a)$$

$$\sigma_{t1} = \frac{6}{H^2} M_{t1} \ ; \qquad 0 \leqslant r \leqslant b, \qquad \ldots (19a)$$

$$\sigma_{t2} = \frac{6}{h^2} M_{t2} \ ; \qquad b \leqslant r \leqslant a, \qquad \ldots (20a)$$

where M_{r1}, M_{r2}, M_{t1}, and M_{t2} are given by equations (17) to (20) respectively.

The deflections and radial moments obtained from equations (15) to (18) have been plotted in Figures 7 to 10, for various $\frac{b}{a}$ and $\frac{H}{h}$ ratios, taking $\frac{h}{a} = 0.1$.

2.7 Discussion

The deflection curves, Figures 7 and 8, show that the deflection obtained from the simplified method is very close to the values obtained from the thin plate theory and the generalized plane stress theory for $\frac{H}{h} = 4$.

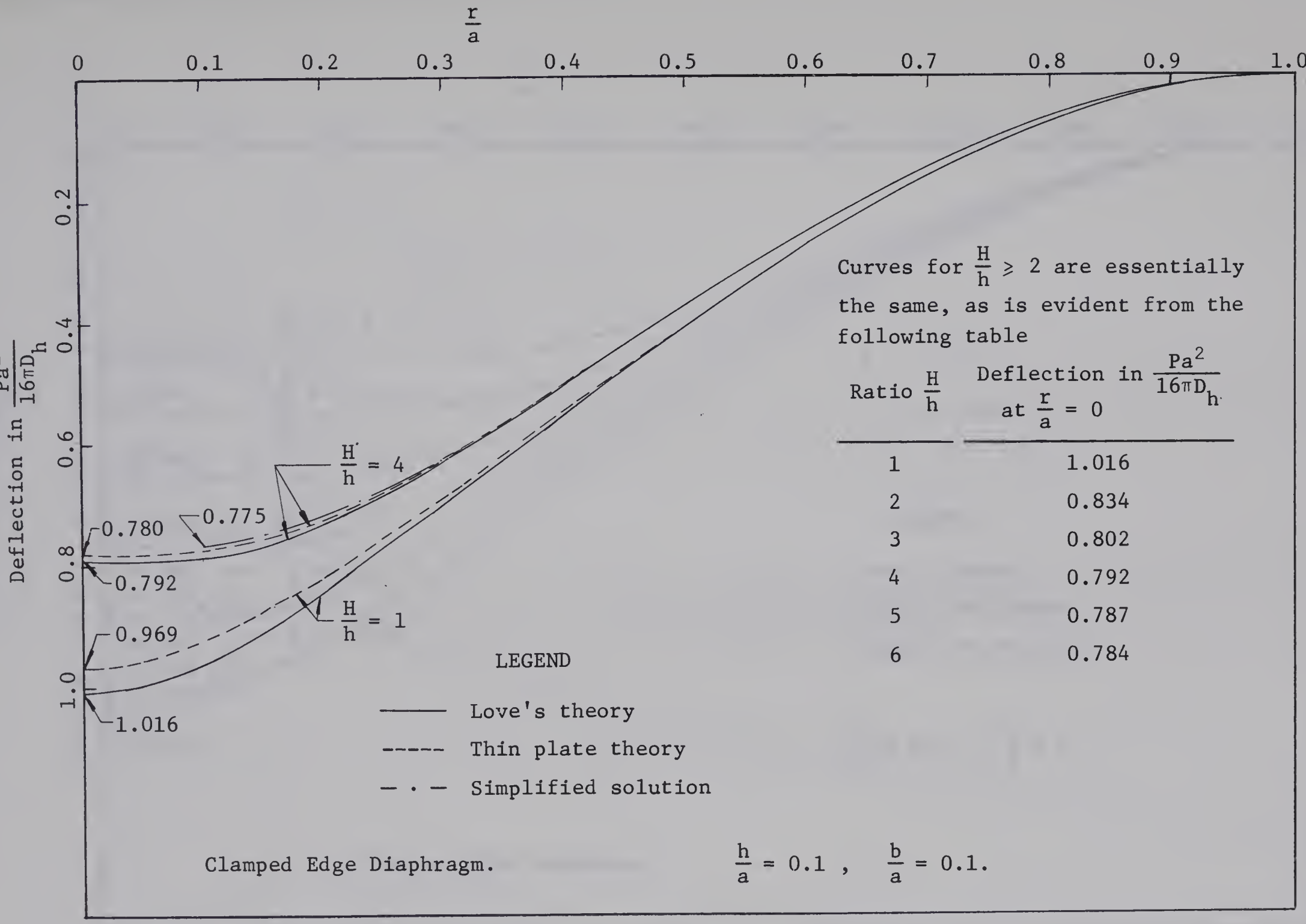

Curves for $\frac{H}{h} \geq 2$ are essentially the same, as is evident from the following table

Ratio $\frac{H}{h}$	Deflection in $\frac{Pa^2}{16\pi D_h}$ at $\frac{r}{a} = 0$
1	1.016
2	0.834
3	0.802
4	0.792
5	0.787
6	0.784

FIGURE 7. Deflection for Different $\frac{H}{h}$ Ratios

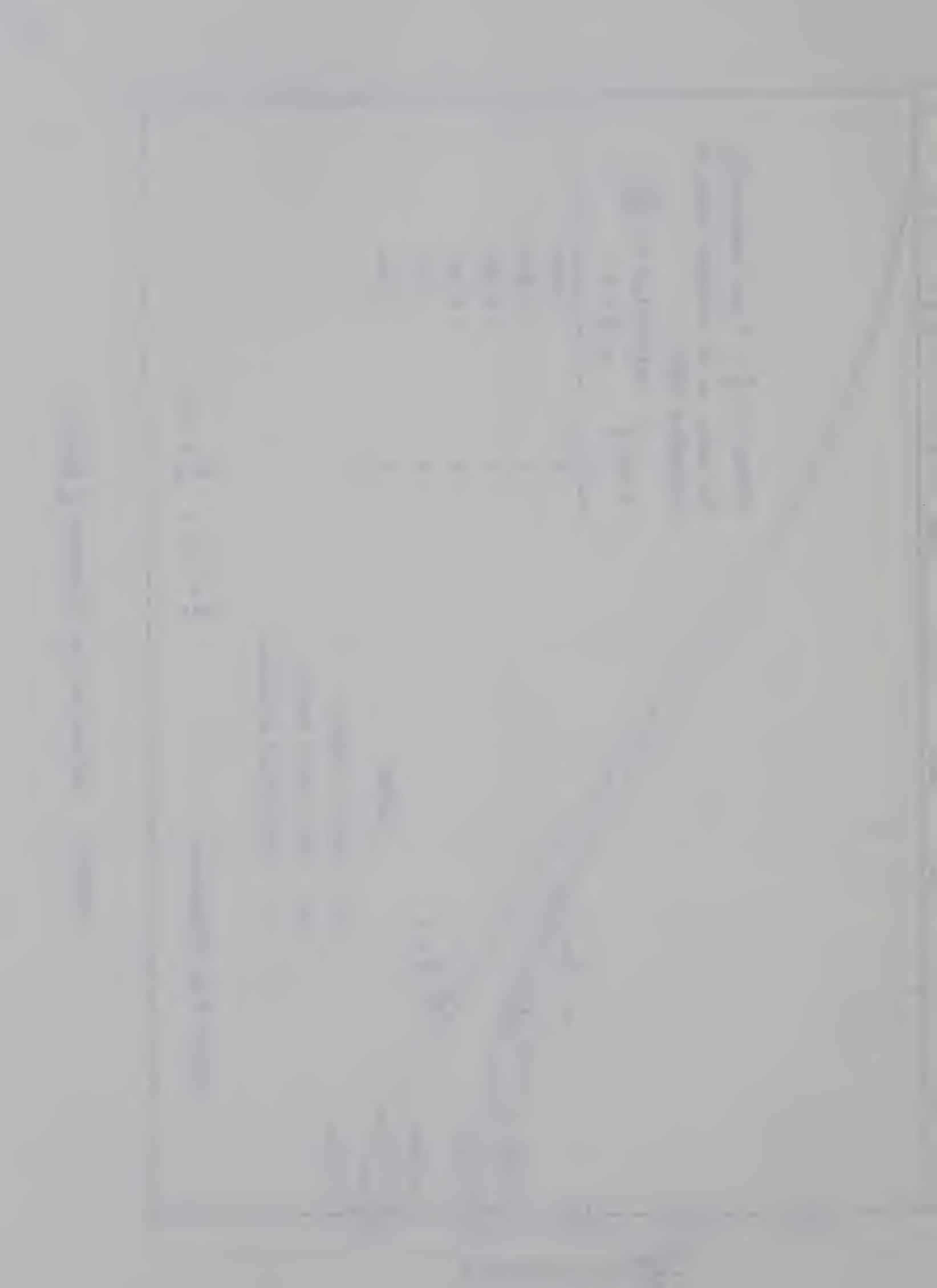

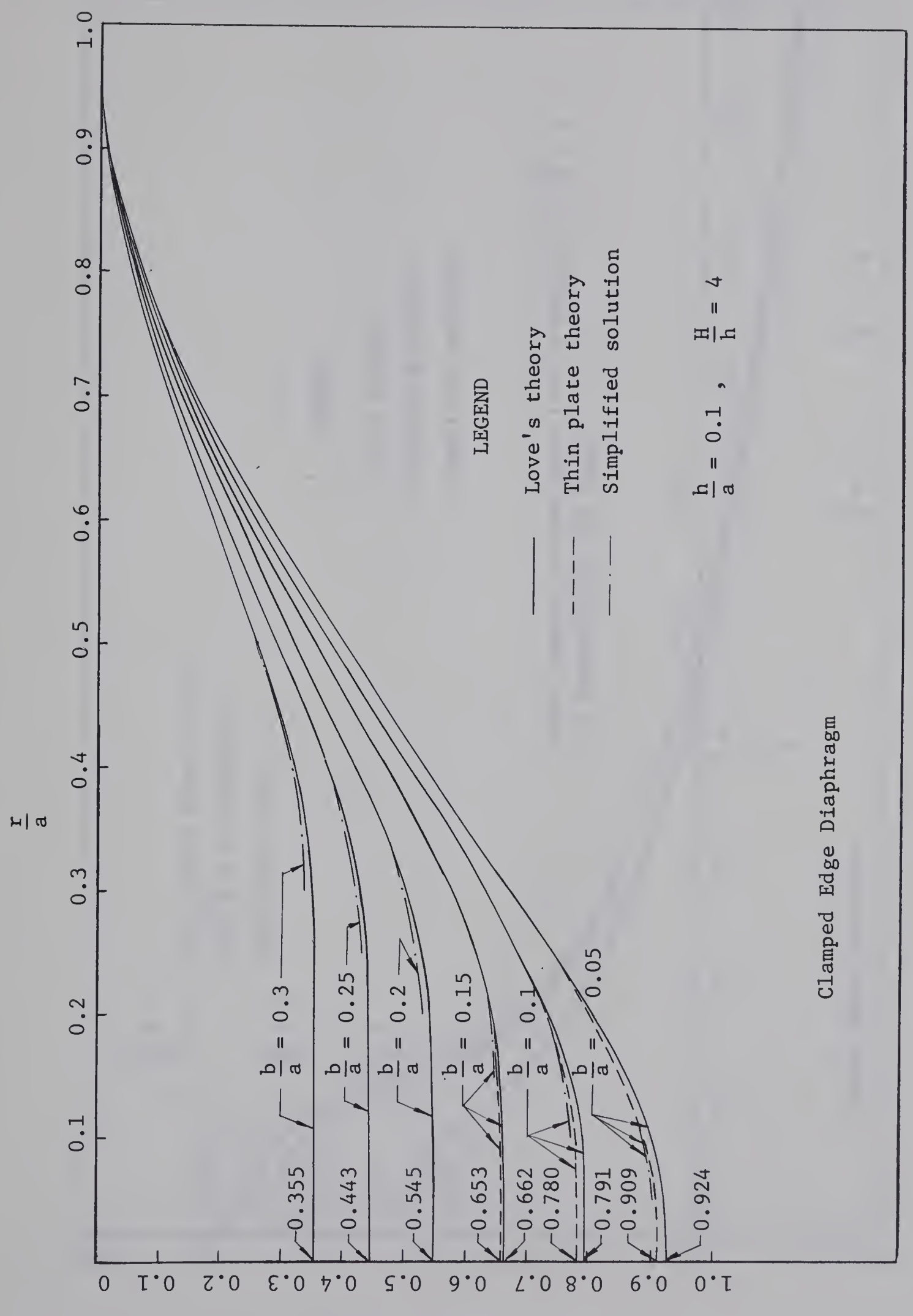

FIGURE 8. Deflection for Different Values of $\frac{b}{a}$

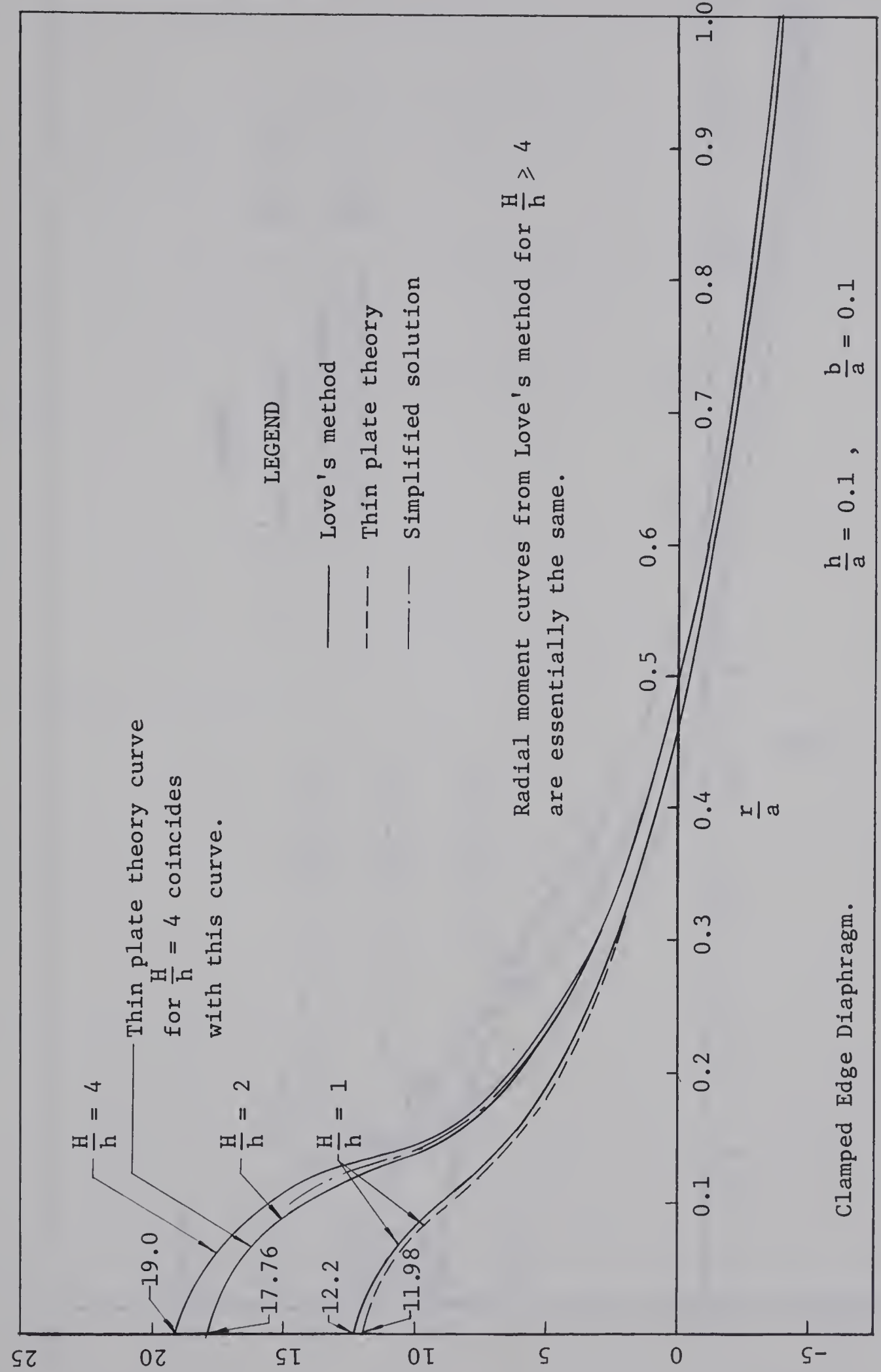

FIGURE 9. Radial Moment for Different $\frac{H}{h}$ Ratios

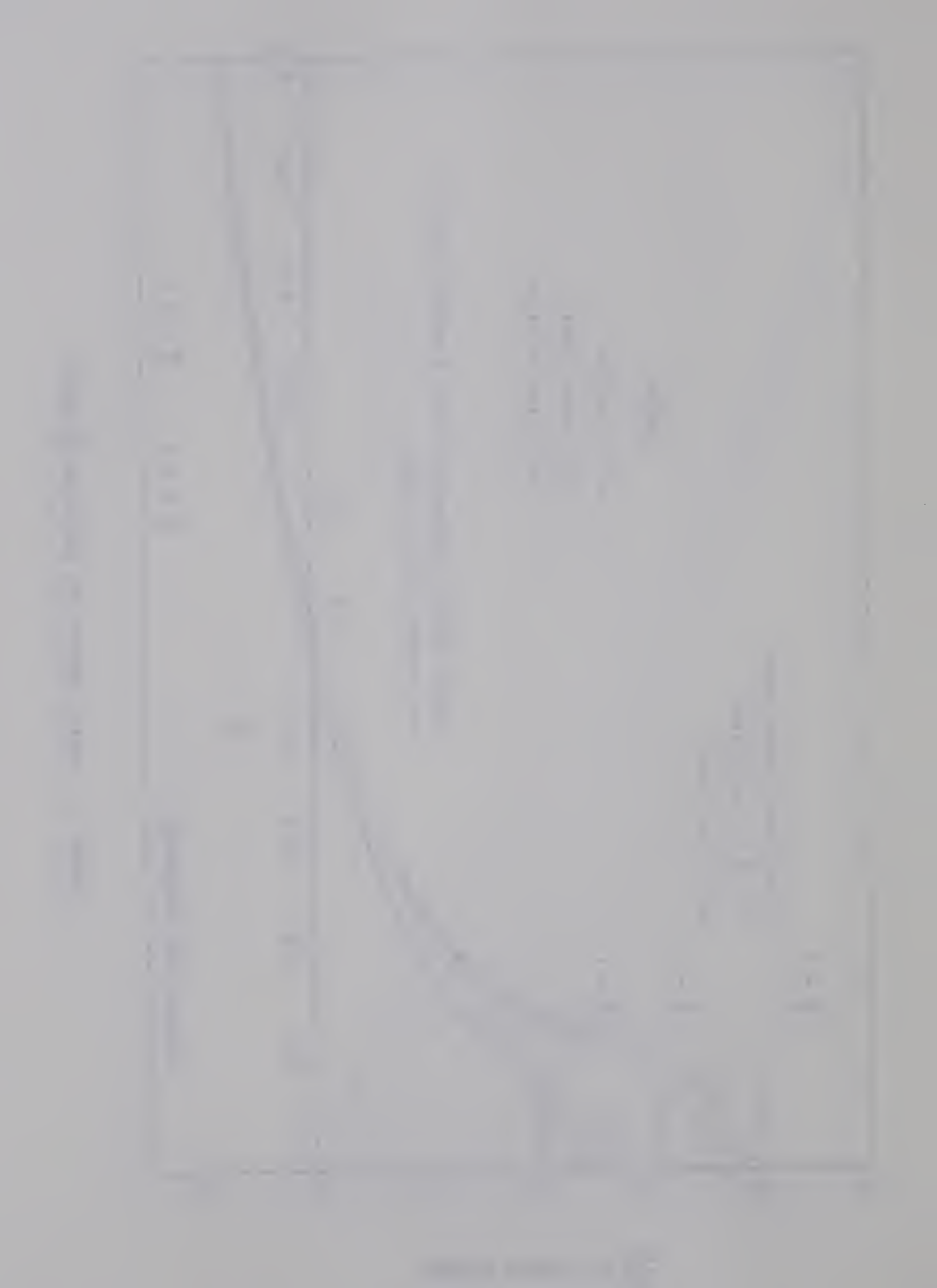

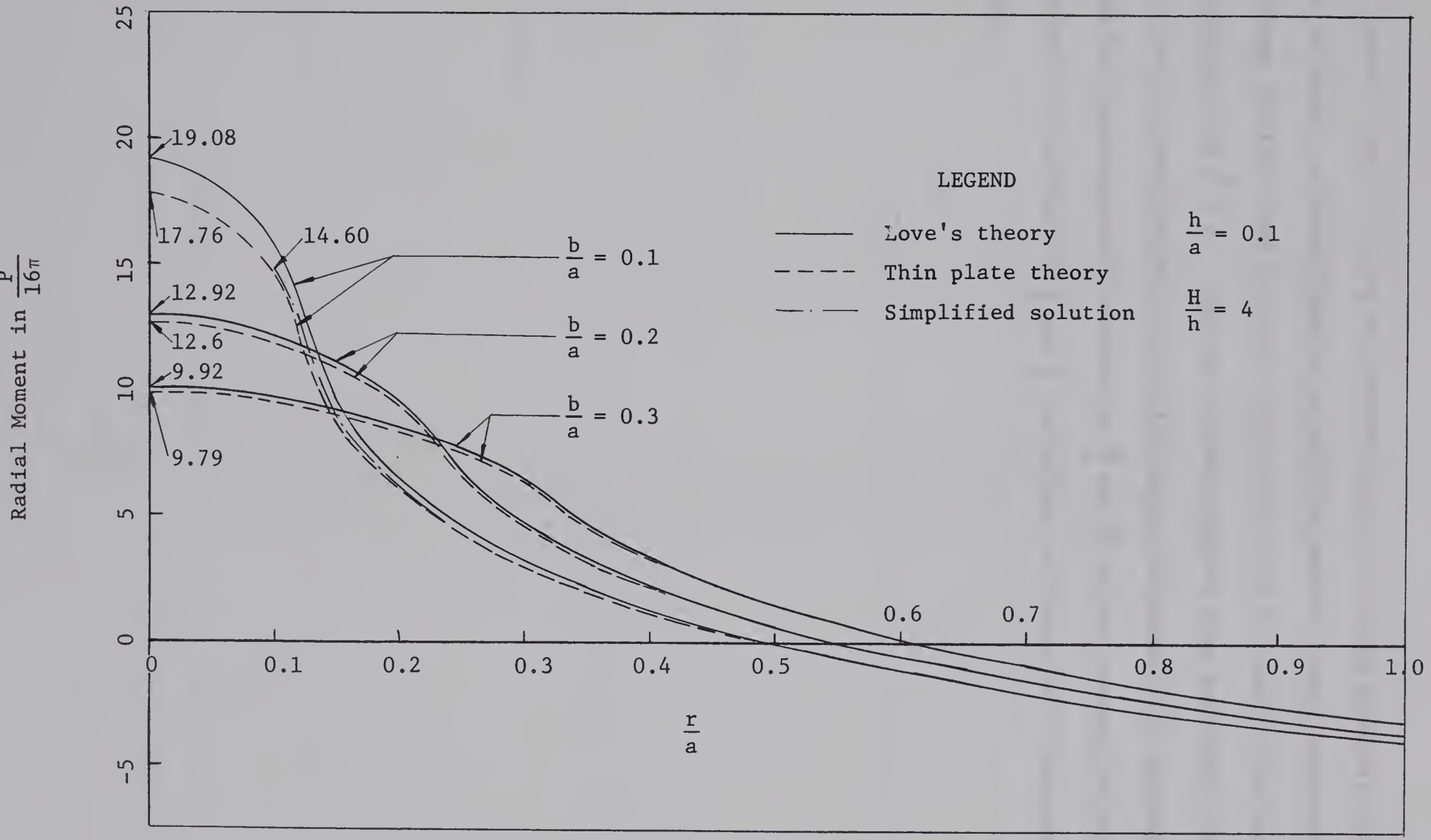

FIGURE 10. Radial Moment for Different $\frac{b}{a}$ Ratios

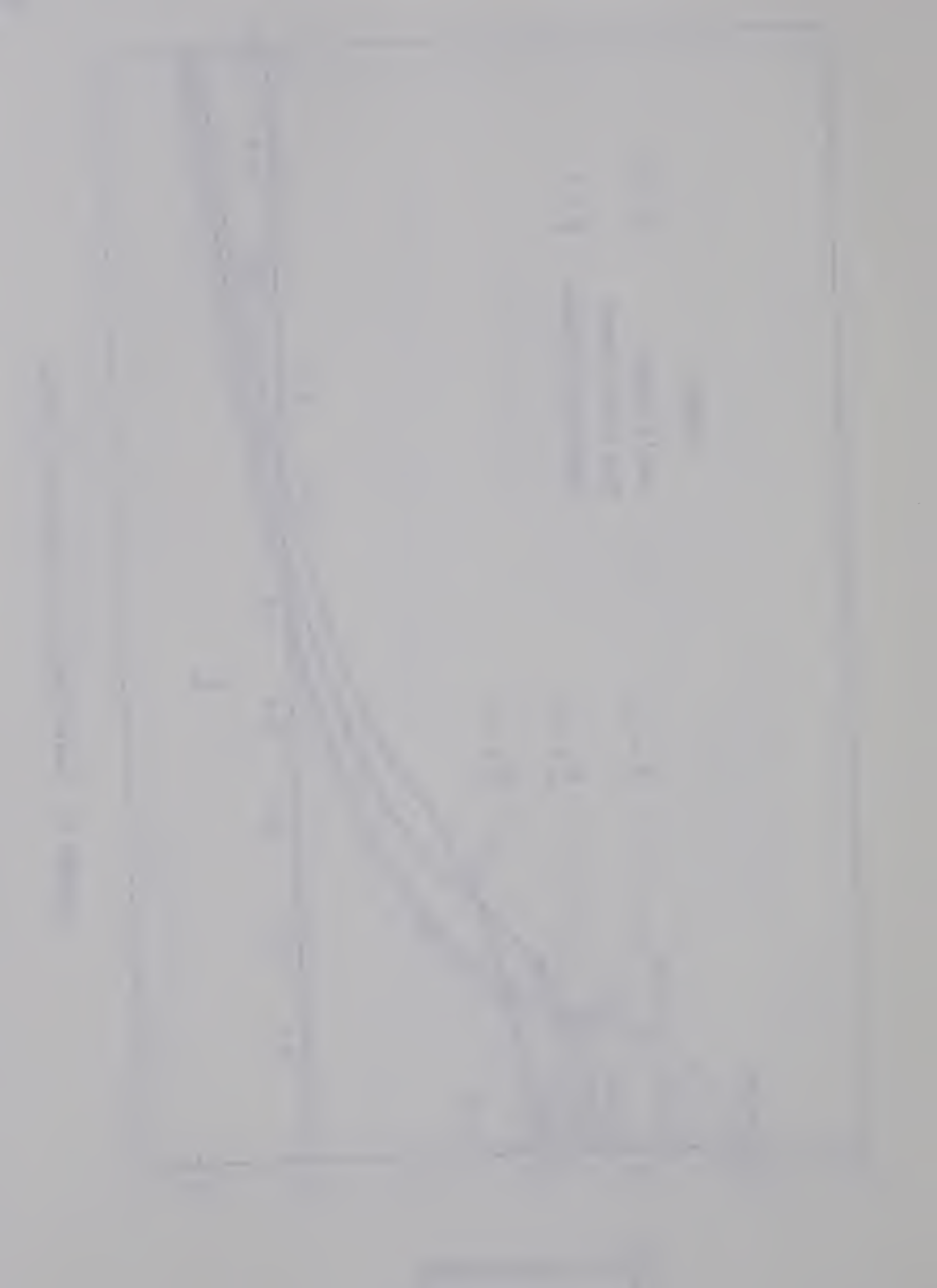

From Figures 9 and 10 it may be observed that the radial moments, hence the radial stresses, obtained from the simplified method closely approximate the values obtained from the thin plate theory and the generalized plane stress theory for $\frac{H}{h} \geqslant 2$. From the values computed from equations (15) to (18) it may be remarked that the radial moment decreases with increase in $\frac{b}{a}$ ratio but increases with increase in $\frac{h}{a}$ and $\frac{H}{h}$ ratios; whereas, deflection decreases with increase in $\frac{b}{a}$ and $\frac{H}{h}$ ratios but increases with increase in $\frac{h}{a}$ ratio.

CHAPTER III

EXPERIMENTS AND RESULTS

3.1 General

In designing the load transducer, the objective was to keep the element as simple as possible. The load was applied in a quasi-static manner in a hydraulic universal testing machine. A special loading head was designed so that when fitted to the existing swivel jointed head, the load was distributed uniformly. Budd strain gauges, type C6-111 having a gauge length of $\frac{1}{16}$ in., were used in connection with a Baldwin-Lima-Hamilton SR-4 strain indicator.

3.2 Stepped-Up Diaphragm

To check the theoretical results, experiments were carried out on two specimens--one having the stepped-up central portion symmetrical about the middle surface and the other with stepping-up only on the top side of the diaphragm.

3.2-1 Symmetrical Diaphragm

The specimen used in the experiment is shown in Figure 11. The strain gauges were fixed on the top and bottom surfaces at radial distances of 0.223 in., 0.5 in., 1.0 in. and 1.25 in., that is, at $\frac{r}{a}$ = 0.148, 0.333, 0.667 and 0.835 respectively. A strain gauge was also placed at the center of the bottom surface. The radial stresses calculated from experimental strains and the theoretically expected stresses at the same points are shown graphically in Figures 12 and 13.

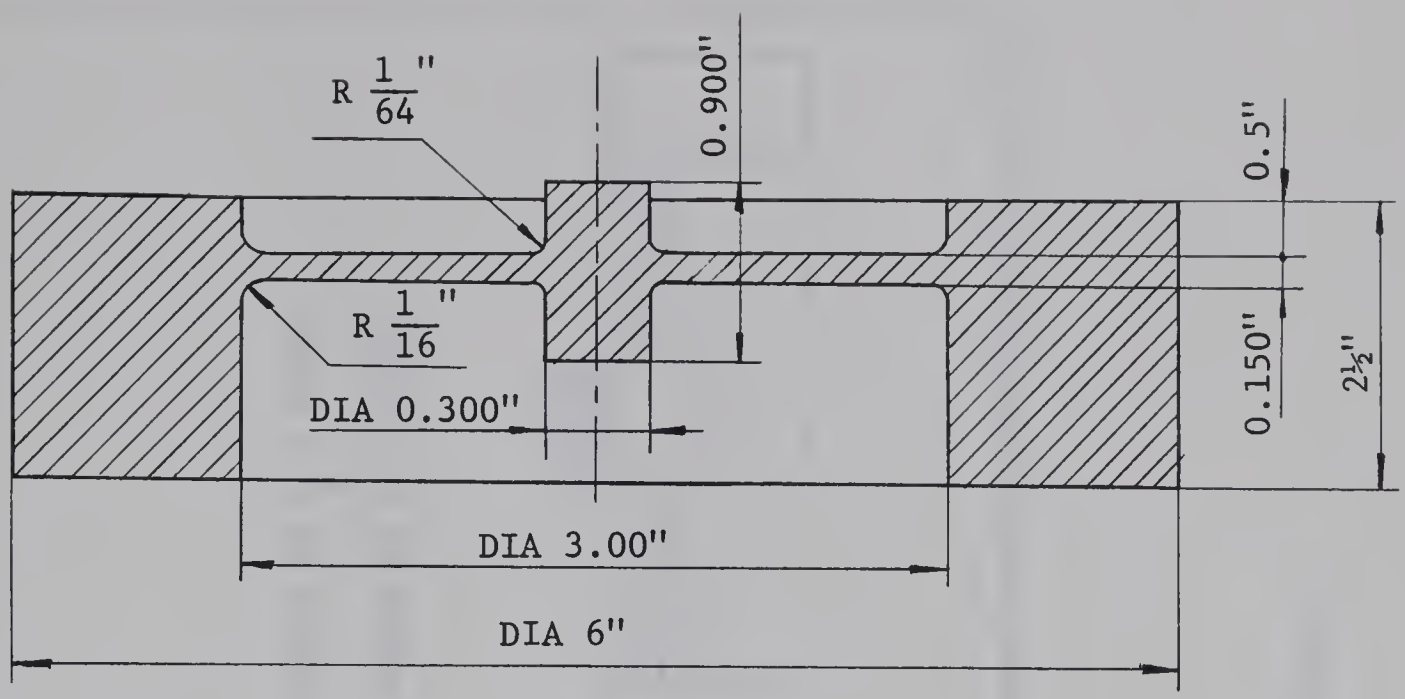

FIGURE 11. Symmetrically Stepped-Up Diaphragm

Discussion:

The thin plate theory and the generalized plane stress theory indicate the existence of radial strains proportional to the bending moment at the center of the bottom surface of the diaphragm. But the strain gauge fixed at the center of the bottom surface did not register any strain, signifying the absence of any bending strain or stress there. This suggests that the plate theories are not applicable to the central region where thickness to radius ratio is high, that is, for $\frac{H}{b} = 6$.

Under the full load, the experimental radial stresses differed from the theoretical stresses by the amounts shown in Table 1. Table 1 shows that the experimental results agree with the theoretical values within tolerable limits only at points away from the central zone.

The experimental stresses showed good linearity with respect to the applied loads, the maximum deviation being 2.6 per cent of the full scale at $\frac{r}{a} = 0.148$.

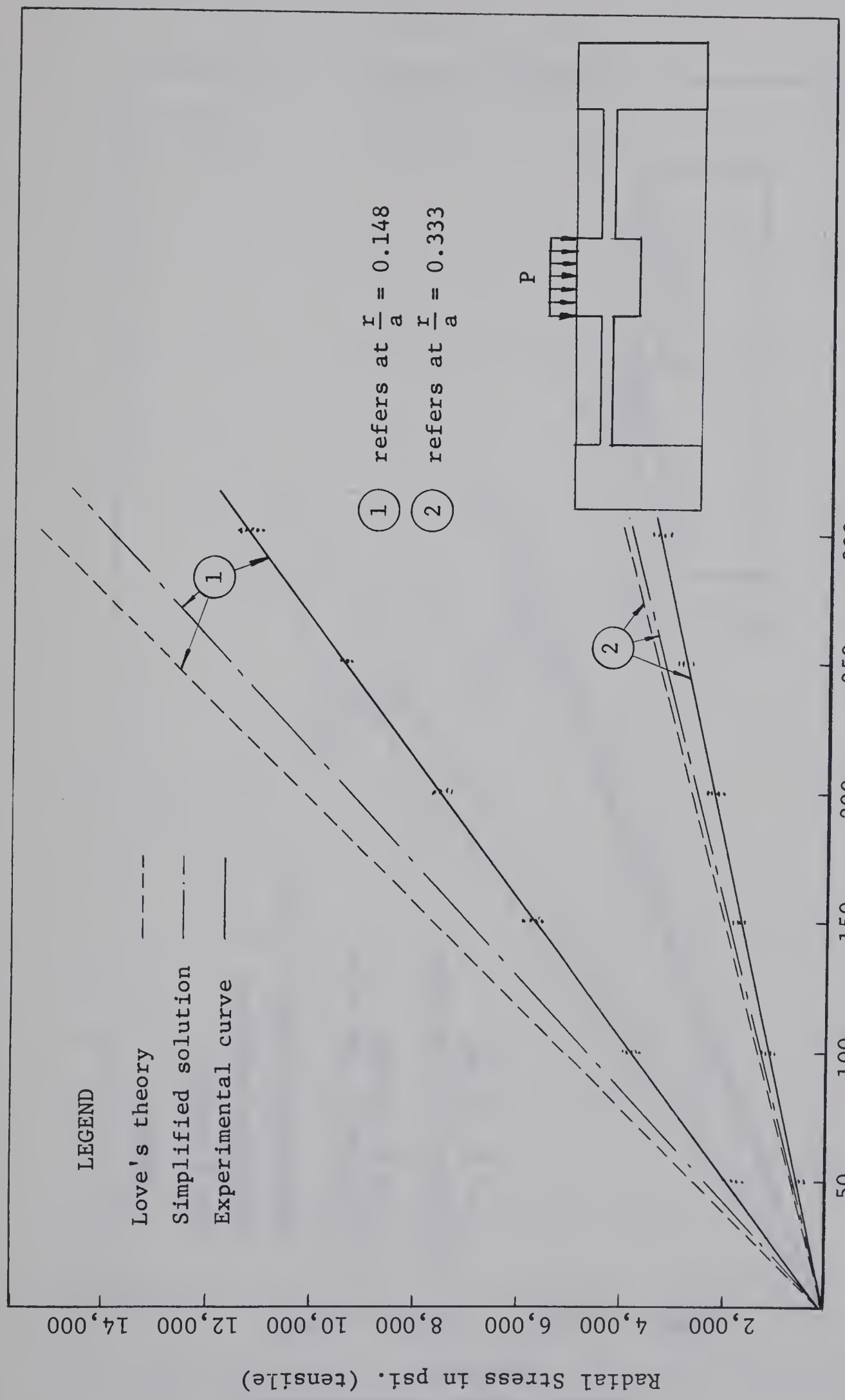

FIGURE 12. Radial Stress vs. Load Curve

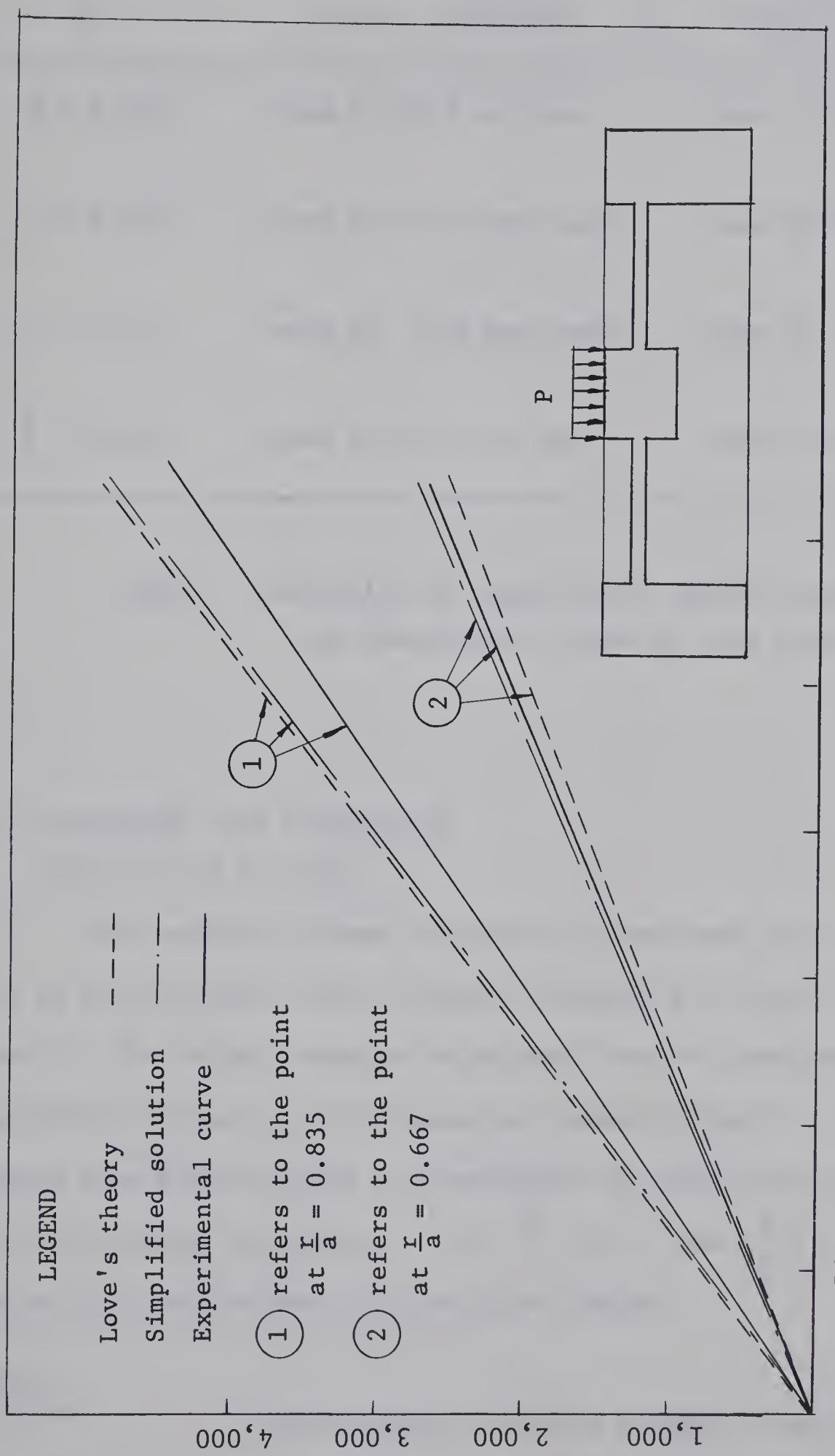

FIGURE 13. Radial Stress vs. Load

At	Deviation from Love's Solution	Deviation from Simplified Solution
$\frac{r}{a} = 0.148$	less by 26.8 per cent	less by 20.5 per cent
$\frac{r}{a} = 0.333$	less by 15.81 per cent	less by 12.7 per cent
$\frac{r}{a} = 0.667$	more by 5.46 per cent	less by 2.9 per cent
$\frac{r}{a} = 0.835$	less by 10.1 per cent	less by 11.8 per cent

TABLE 1. Deviation of Experimental Radial Stress from the Theoretical Stress at Full Load

3.2-2 Diaphragm with Stepping-Up Only on the Top Side

The specimen, shown in Figure 14a, was used in this experiment. It is to be noted that this specimen corresponds in shape to one shown in Figure 2. The radial stresses calculated from the experimental results along with the theoretical stresses are shown in Table 2. The theoretical stresses have been obtained from equations (9) and (10), derived from the thin plate theory, by taking $a = 2''$, $\frac{b}{a} = 0.1$, and $\frac{H}{h} = 4$, and from the equation (2) derived from the simplified method.

Remarks:

Experimentally obtained stresses showed linearity within allowable limits. At the edge, $\frac{r}{a} = 0.89$, the experimental radial

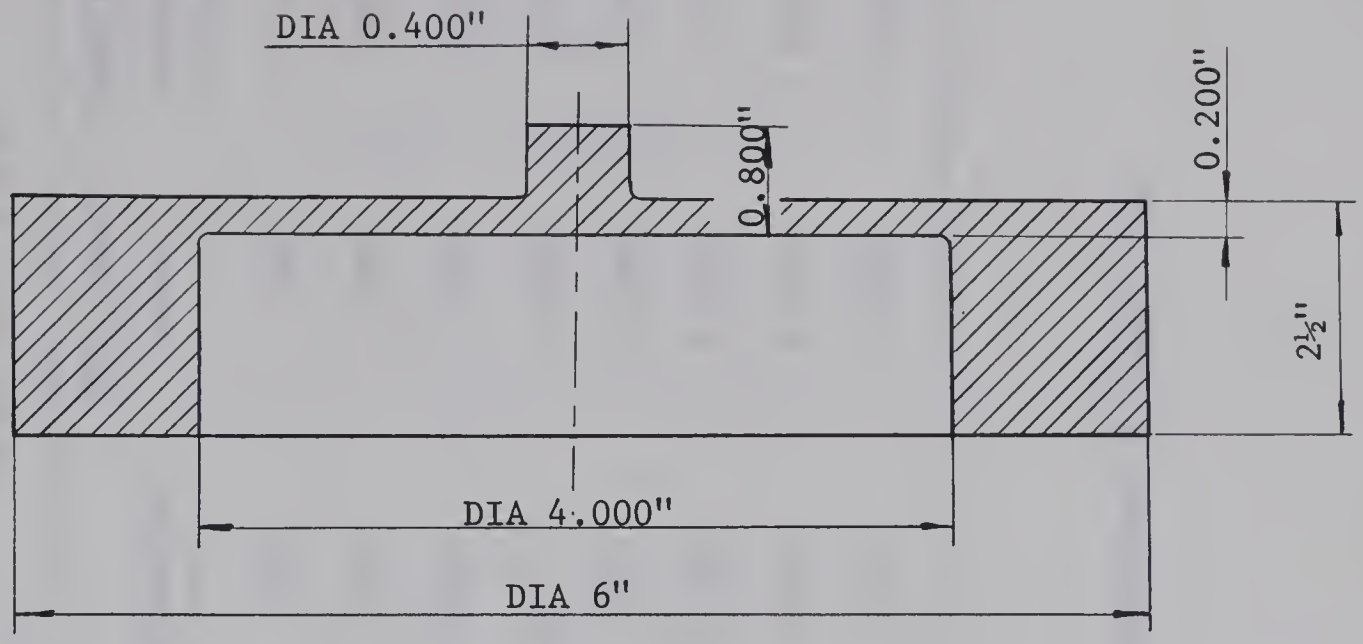

FIGURE 14a. Asymmetrical Diaphragm

stress was one per cent higher than that obtained from the simplified method and about seven per cent higher than that predicted from thin plate theory. However, for the central region the theoretical and experimental stresses differed considerably.

Load in lbs.	Radial stress in psi at $\frac{r}{a} = 0$		Radial stress in psi at $\frac{r}{a} = 0.133$			Radial stress in psi at $\frac{r}{a} = 0.89$		
	Experimental	Thin plate theory	Experimental	Thin plate theory	Simplified method	Experimental	Thin plate theory	Simplified method
100	1,687	331	2,553	3,450	3,280	- 964	- 900	- 952
200	3,388	662	5,055	6,900	6,560	- 1,891	- 1,800	- 1,905
300	4,139	993	7,562	10,350	9,840	- 2,880	- 2,700	- 2,857
400	6,765	1,325	10,125	13,800	13,120	- 3,847	- 3,600	- 3,810
500	8,512	1,655	12,512	17,200	16,400	- 4,750	- 4,500	- 4,762
600	10,217	1,986	15,012	20,700	19,680	- 5,742	- 5,400	- 5,715
700	11,892	2,318	18,562	24,150	22,960	- 6,682	- 6,300	- 6,667
800	13,737	2,650	20,232	27,600	26,240	- 7,697	- 7,200	- 7,640

TABLE 2. Experimental and Theoretical Radial Stresses for the Diaphragm of Figure 14a

CHAPTER IV

CONCLUSION (PART A)

In order to determine the stresses and strains for the diaphragms shown in Figures 1 and 2, the shape of the diaphragm was idealized to a symmetrical section as shown in Figure 5. But the experimental results, shown in Table 2, did not agree with those obtained from the idealized shape except at $\frac{r}{a} = 0.89$. It may be concluded that the idealization suggested by Hoeland[10] does not give the desired results in the vicinity of the idealized zone. The experimental results indicate that the non-symmetrically stepped-up central zone sets up a "disturbing stress field." For regions far away from the stepped-up zone (about eight times the radius of the boss in this experiment) the stress distribution can be predicted by idealizing the shape as suggested by Hoeland and discussed in Sections 2.5 and 2.6.

The results obtained suggest that the solution obtained by the simplified method gives a better approximation to the actual stress distribution than the thin plate theory and Love's theory when $\frac{H}{h}$ ratio is large (four to six in the conducted experiments). The disadvantage of the simplified method is that it does not give any information about the moment or stress distribution and the deflection in the region $0 \leqslant r \leqslant b$.

It is felt, only a rigorous method as suggested in Section 2.3 may give a better estimate of the actual stresses and strains in the diaphragm.

The experiment on the diaphragm with a symmetrical section shows that though the actual stress is somewhat less than that predicted by the theories considered, these theories give a fair estimate of the stresses.

Hence, moderately thick plate theory may be used for optimizing the dimensions of the diaphragm to design a load transducer.

PART B

OPTIMIZATION AND DESIGN PROCEDURE FOR A DIAPHRAGM TYPE LOAD TRANSDUCER

CHAPTER V

OPTIMIZATION OF DIMENSIONS OF DIAPHRAGM

5.1 Optimization

The load transducer under consideration converts the load-induced mechanical strains to electrical signals by means of a Wheatstone bridge. The sensitivity of the transducer is a function of the strain measured by the electrical resistance strain gauges. On the other hand, an ideal load transducer measures the load without undergoing any deformation itself. These two ideas contradict each other. Furthermore, for some transducer applications the diaphragm would be designed so that the applicable load is a maximum for a given allowable stress of the material of the diaphragm. In the present work, the latter criterion has been taken as the basis of optimization for design purposes. The sensitivity will then mainly depend on the characteristics of the electrical circuitry.

Figures 9 and 10 show that the bending moment at the junction of the two thicknesses is not much lower than that at the center. At the junction, the bending stress considered for the zone $b \leqslant r \leqslant a$ is considerably higher because of the small thickness than the bending stress in the zone $0 \leqslant r \leqslant b$. Hence, optimization is made by taking the stress at radius $r = b$ and for thickness equal to h as the critical stress. From equation (17) the radial moment at $r = b$ is given by

$$M_r = \frac{P}{16\pi}\left[-(3+\mu) + 2\alpha\,(1+\mu)\,\overline{B}_1 - \frac{8+\mu+\mu^2}{5(1-\mu)}\,\frac{H^2}{b^2}\right].$$

The radial stress at $r = b$ due to this moment M_r is

$$\sigma_r = \frac{6Mr}{h^2} = \frac{3P}{8\pi h^2}\left[-(3+\mu) + 2\alpha(1+\mu)\overline{B}_1 - \frac{8+\mu+\mu^2}{5(1-\mu)} \cdot \frac{H^2}{b^2}\right]$$

Thus,

$$P = \frac{8\pi a^2}{3}\sigma_r \frac{h^2}{a^2} \frac{1}{\left[-(3+\mu) + 2\alpha(1+\mu)\overline{B}_1 - \frac{8+\mu+\mu^2}{5(1-\mu)} \cdot \frac{H^2}{b^2}\right]}$$

For an allowable stress σ_r, depending upon the material of the diaphragm, and a given outside radius $r = a$, the load P will be a maximum when the expression

$$\frac{h^2}{a^2} \frac{1}{\left[-(3+\mu) + 2\alpha(1+\mu)\overline{B}_1 - \frac{8+\mu+\mu^2}{5(1-\mu)} \cdot \frac{H^2}{b^2}\right]} \qquad \ldots (21)$$

is a maximum.

A computer was used to obtain the values of the parameters $\frac{h}{a}$, $\frac{b}{a}$, and $\frac{H}{h}$, for which expression (21) is a maximum. The following data were programmed into an IBM 360 computer:

Values of $\frac{b}{a}$ from 0.05 to 0.3 in 6 steps,

Values of $\frac{h}{a}$ from 0.01 to 0.6 in 60 steps,

and Values of $\frac{H}{h}$ from 1 to 6 in 6 steps.

The result obtained was that the applicable load is a maximum when

$$\frac{b}{a} = 0.3, \qquad \frac{h}{a} = 0.6, \qquad \frac{H}{h} = 1.0.$$

This means that:

1) The diaphragm should be uniformly thick without any stepping-up, since $\frac{H}{h} = 1.0$.
2) The diaphragm should be thick, as a large $\frac{h}{a}$ ratio gives a maximum load which is indicated by the result $\frac{h}{a} = 0.6$.
3) The load should be distributed over an area as large as possible because of the result $\frac{b}{a} = 0.3$ (the maximum value which was programmed).

Remarks:

In view of the above optimization and the stress concentration, which will evidently be introduced at the junction of the thicknesses, a uniform thickness throughout the diaphragm is recommended for a transducer application. The load, therefore, is to be applied on the diaphragm through a projection under the loading plate rather than having the projection as an integral part of the diaphragm.

Since both the thin plate theory and the moderately thick plate theory do not agree completely with the experimental results, it was decided to use the thin plate theory, equations (7) to (12), in the design procedure because it led to an easier analysis.

5.2 Uniformly Thick Diaphragm--Thin Plate Theory

For a uniformly thick diaphragm the equations (7) to (12) reduce to the following forms (by letting H be equal to h):

$$w_1 = \frac{qb^4}{64D_h}\left[\left(\frac{r}{b}\right)^4 + 4\,\frac{a^2}{b^2} - 3 + 4\,\ln\frac{b}{a} + 2\left(\frac{r}{b}\right)^2\left(4\,\ln\frac{b}{a} - \frac{b^2}{a^2}\right)\right];$$

$$0 \leqslant r \leqslant b \qquad \ldots (22)$$

$$w_2 = \frac{qa^2b^2}{16D_h}\left[\left(1 + \frac{b^2}{2a^2}\right)\left(1 - \frac{r^2}{a^2}\right) + \left(\frac{b^2}{a^2} + \frac{2r^2}{a^2}\right)\ln\frac{r}{a}\right] \quad ;$$

$$b \leqslant r \leqslant a, \qquad \ldots (23)$$

$$M_{r1} = -\frac{qb^2}{16}\left[\frac{r^2}{b^2}(3 + \mu) + (1 + \mu)\left(4\ln\frac{b}{a} - \frac{b^2}{a^2}\right)\right] \quad ;$$

$$0 \leqslant r \leqslant b, \qquad \ldots (24)$$

$$M_{r2} = -\frac{qb^2}{16}\left[4(1 + \mu)\ln\frac{r}{a} + 2(3 + \mu) - \left(2 + \frac{b^2}{a^2}\right)(1 + \mu) - \frac{b^2}{r^2}(1 - \mu)\right];$$

$$b \leqslant r \leqslant a, \qquad \ldots (25)$$

$$M_{t1} = -\frac{qb^2}{16}\left[\frac{r^2}{b^2}(1 + 3\mu) + (1 + \mu)\left(4\ln\frac{b}{a} - \frac{b^2}{a^2}\right)\right] \quad ;$$

$$0 \leqslant r \leqslant b, \qquad \ldots (26)$$

$$M_{t2} = -\frac{qb^2}{16}\left[4(1 + \mu)\ln\frac{r}{a} + 2(1 + 3\mu) - \left(2 + \frac{b^2}{a^2}\right)(1 + \mu) + \frac{b^2}{r^2}(1 - \mu)\right];$$

$$b \leqslant r \leqslant a, \qquad \ldots (27)$$

$$\sigma_{r1} = \frac{6}{h^2} M_{r1}, \qquad 0 \leqslant r \leqslant b, \qquad \ldots (24a)$$

$$\sigma_{r2} = \frac{6}{h^2} M_{r2}, \qquad b \leqslant r \leqslant a, \qquad \ldots (25a)$$

$$\sigma_{t1} = \frac{6}{h^2} M_{t1}, \qquad 0 \leqslant r \leqslant b, \qquad \ldots (26a)$$

$$\sigma_{t2} = \frac{6}{h^2} M_{t2}, \qquad b \leqslant r \leqslant a, \qquad \ldots (27a)$$

where M_{r1}, M_{r2}, M_{t1}, and M_{t2} are given by equations (24) to (27) respectively.

CHAPTER VI

DESIGN PROCEDURE FOR A DIAPHRAGM TYPE LOAD TRANSDUCER

This chapter discusses a design procedure for a load transducer having a diaphragm type element and using a bonded electrical resistance strain gauge. The general requirements of a load transducer may be stated as follows:

a) high sensitivity,

b) small size, low mass, high natural frequency,

c) adequate strength,

d) wide load range,

e) linear response.

In connection with sensitivity and linear response the design of the transducer depends on the selection of the type of the strain gauges and associated electrical circuitry. Wenk[4] recommended the use of rectangular gauges in place of spiral strain gauges because of the latter's undesirable properties of non-linearity of response, hysteresis and poor temperature compensation. On the other hand, Werner[5] suggested using spiral type strain gauges because of their advantages of small size, high sensitivity and high natural frequency. Werner traced the cause of the undesirable properties of spiral gauges, as reported by Wenk, to the failure of the innermost turns of the spiral to follow the strains because of their small radius of curvature. He, therefore, suggested leaving out the winding of the gauge near the central region. In this investigation both types of gauges were used to compare their performances. The design procedure used in this chapter is similar to that which was used by Werner[5] in designing

pressure transducers.

Radial strain e_r and tangential strain e_t, from the laws of elasticity, are given by

$$e_r = \frac{1}{E}(\sigma_r - \mu\sigma_t) = \frac{6}{Eh^2}(M_r - \mu M_t)$$

$$e_t = \frac{1}{E}(\sigma_t - \mu\sigma_r) = \frac{6}{Eh^2}(M_t - \mu M_t) \ .$$

Substituting the values of M_r and M_t from equations (24) to (27) in these two equations, we obtain

$$e_{r1} = -\frac{3}{8}\frac{qb^2}{Eh^2}(1 - \mu^2)\left[3\frac{r^2}{b^2} + 4\ln\frac{b}{a} - \frac{b^2}{a^2}\right] ;$$

$$0 \leqslant r \leqslant b, \qquad \ldots (28)$$

$$e_{t1} = -\frac{3}{8}\frac{qb^2}{Eh^2}(1 - \mu^2)\left[\frac{r^2}{b^2} + 4\ln\frac{b}{a} - \frac{b^2}{a^2}\right] ;$$

$$0 \leqslant r \leqslant b, \qquad \ldots (29)$$

$$e_{r2} = -\frac{3}{8}\frac{qb^2}{Eh^2}(1 - \mu^2)\left[4\ln\frac{r}{a} + 4 - \frac{b^2}{r^2} - \frac{b^2}{a^2}\right] ;$$

$$b \leqslant r \leqslant a,$$

$$e_{t2} = -\frac{3}{8}\frac{qb^2}{Eh^2}(1 - \mu^2)\left[\frac{b^2}{r^2} + 4\ln\frac{r}{a} - \frac{b^2}{a^2}\right] ;$$

$$b \leqslant r \leqslant a \ .$$

CHAPTER VI

DESIGN PROCEDURE FOR A DIAPHRAGM TYPE LOAD TRANSDUCER

This chapter discusses a design procedure for a load transducer having a diaphragm type element and using a bonded electrical resistance strain gauge. The general requirements of a load transducer may be stated as follows:

a) high sensitivity,

b) small size, low mass, high natural frequency,

c) adequate strength,

d) wide load range,

e) linear response.

In connection with sensitivity and linear response the design of the transducer depends on the selection of the type of the strain gauges and associated electrical circuitry. Wenk[4] recommended the use of rectangular gauges in place of spiral strain gauges because of the latter's undesirable properties of non-linearity of response, hysteresis and poor temperature compensation. On the other hand, Werner[5] suggested using spiral type strain gauges because of their advantages of small size, high sensitivity and high natural frequency. Werner traced the cause of the undesirable properties of spiral gauges, as reported by Wenk, to the failure of the innermost turns of the spiral to follow the strains because of their small radius of curvature. He, therefore, suggested leaving out the winding of the gauge near the central region. In this investigation both types of gauges were used to compare their performances. The design procedure used in this chapter is similar to that which was used by Werner[5] in designing

Theoretically a spiral strain gauge measures the average tangential strain over the area on which it is fixed. To facilitate calculation of the average strain, the radius of the spiral gauge, R, is kept less than b, so that only one equation for tangential strain, e_{t1}, is required. The average tangential strain under the spiral gauge of radius R < b is given by the formula

$$\bar{e}_t = \frac{1}{R} \int_o^R e_{t1} dr \ .$$

Using equation (29) for e_{t1} in this, the equation becomes

$$\bar{e}_t = - \frac{3}{8} \frac{qb^2}{Eh^2} (1 - \mu^2) \left[\frac{R^2}{3b^2} + 4 \ln \frac{b}{a} - \frac{b^2}{a^2} \right] . \qquad \ldots (30)$$

Design Equations

a) The stress and strain equations derived from the thin plate theory require that the ratio of thickness to radius of the diaphragm to be small. For a moderate estimate, Werner suggested

$$\frac{h}{a} \leqslant \frac{2}{5} . \qquad \ldots (31)$$

b) For linearity, the maximum deflection of the plate should be a small fraction of the thickness. From experiments Wenk found that $w < \frac{h}{3}$ ensures linearity. On this premise, the substitution of equation (22) for w_1 with r = 0 results in the condition

$$\frac{h}{a} \geqslant \sqrt[4]{\frac{9}{16} \frac{q_{max}}{E} \frac{b^4}{a^4} (1 - \mu^2) \left[4 \frac{a^2}{b^2} + 4 \ln \frac{b}{a} - 3 \right]} . \qquad \ldots (32)$$

c) For adequate sensitivity, the strain gauge should give a certain minimum output $\bar{e}_{t_{min}}$ at q_{min}. This gives rise to the following equation:

$$\frac{\bar{e}_t}{q} \geqslant \frac{\bar{e}_{t_{min}}}{q_{min}} .$$

On substitution of the value of $\bar{e}_t$ from equation (30) it follows:

$$\frac{h}{a} \leqslant \sqrt{\frac{3}{8} \frac{b^2}{a^2} \frac{q_{min}}{\bar{e}_{t_{min}}} \frac{(1 - \mu^2)}{E} \left[\frac{b^2}{a^2} - 4 \ln \frac{b}{a} - \frac{R^2}{3b^2}\right]} \quad . \qquad \ldots (33)$$

d) The bending moment of a uniformly thick diaphragm is a maximum at the center (as is evident from Figure 9 from the curve for $\frac{H}{h} = 1$), making the tensile bending stress, at the center of the bottom surface, the critical stress for design. The maximum bending moment from equation (24) with $\frac{r}{a} = 0$ is

$$M_{r_{max}} = - \frac{qb^2}{16} (1 + \mu) \left[4 \ln \frac{b}{a} - \frac{b^2}{a^2}\right] .$$

Therefore, $\sigma_{r_{max}} = - \frac{3}{8} \frac{qb^2}{h^2} (1 + \mu) \left[4 \ln \frac{b}{a} - \frac{b^2}{a^2}\right] .$

If the diaphragm is to have adequate strength at the maximum pressure q_{max}, then for a factor of safety of two

$\sigma_{r_{max}} \leqslant \frac{\sigma_1}{2}$, where σ_1 is the maximum working stress of the diaphragm material.

Substituting the value of $\sigma_{r_{max}}$ in this inequality, the result is

$$\frac{h}{a} \geq \sqrt{\frac{3}{4} \frac{q_{max}}{\sigma_1} \frac{b^2}{a^2} (1 + \mu) \left[\frac{b^2}{a^2} - 4 \ln \frac{b}{a}\right]} \quad . \qquad \ldots (34)$$

e) In practice the lowest natural frequency, f, of the diaphragm is kept much higher than f_L, the expected frequency of the load transient. Therefore,

$$f > f_L$$

The lowest natural frequency of a clamped edge diaphragm is given by Morse[13] as the following expression:

$$f = 0.467 \frac{h}{a^2} \sqrt{\frac{Eg}{\gamma(1 - \mu^2)}} \quad \text{cps} .$$

Thus,

$$\frac{h}{a} > \frac{f_L \cdot a}{0.467} \sqrt{\frac{\gamma(1 - \mu^2)}{g \cdot E}} \quad . \qquad \ldots (35)$$

To facilitate designing, equations (31) to (35) are plotted in a graph taking a fixed value of $\frac{b}{a}$, which is generally determined by the loading conditions. A set of graphs corresponding to equations (31) to (35) for $\frac{b}{a} = 0.1$ is shown in Figure 14. The following values for physical constants were chosen for plotting the graphs:

$\mu = 0.3$; $E = 29 \times 10^6$ psi; $\gamma = 0.308$ lb/cu-inch;

$\sigma_1 = 30{,}000$ psi, 50,000 psi, and 80,000 psi;

$\frac{R}{a} = 0$ and 0.1 .

For rectangular gauges $\frac{R}{a} = 0$. The value of $\bar{e}_{t_{min}}$ was chosen as 1.0 μ-in./in. for plotting the sensitivity equation (33). The sensitivity graphs in Figure 14 are applicable without any correction if $\bar{e}_{t_{min}}$ is 1.0 μ-in./in. If another value is used, a modified value of q_{min} obtained by dividing the actual q_{min} through the desired $\bar{e}_{t_{min}}$ expressed in μ-in./in. must be used.

The region of satisfactory design of a diaphragm is shown by the arrows in Figure 14. The pressures indicated by the intersection points of a horizontal line, corresponding to a fixed $\frac{h}{a}$ ratio, with the sensitivity line on the left and with the strength line or deflection line on the right denote the minimum and maximum pressures for which the diaphragm is optimum. The use of the graphs for designing a diaphragm is shown by the following example.

Example Using Figure 14

A diaphragm type transducer is to be designed for a load range of 50 to 2000 lb. From the space available, radius "a" may be taken as 1.5 in. and the load will be distributed uniformly over a radius of 0.15 in. Ordinary rectangular gauges are to be used. The allowable stress of the diaphragm material is $\sigma_1 = 50{,}000$ psi.

The object of the design is to find out an optimum thickness "h" of the diaphragm.

As "b" is given to be 0.15 in., the ratio $\frac{b}{a} = 0.1$. The area under load is $\pi b^2 = 0.0706$ sq. in. Corresponding to the load range of 50 to 2000 lb, the pressure range for which the design is to be made is $\frac{50}{0.0706}$ to $\frac{2000}{0.0706}$ psi. or 706 to 28,200 psi.

A vertical line is drawn at 28,200 psi on the pressure axis of the design chart, Figure 14. The vertical line cuts the strength line

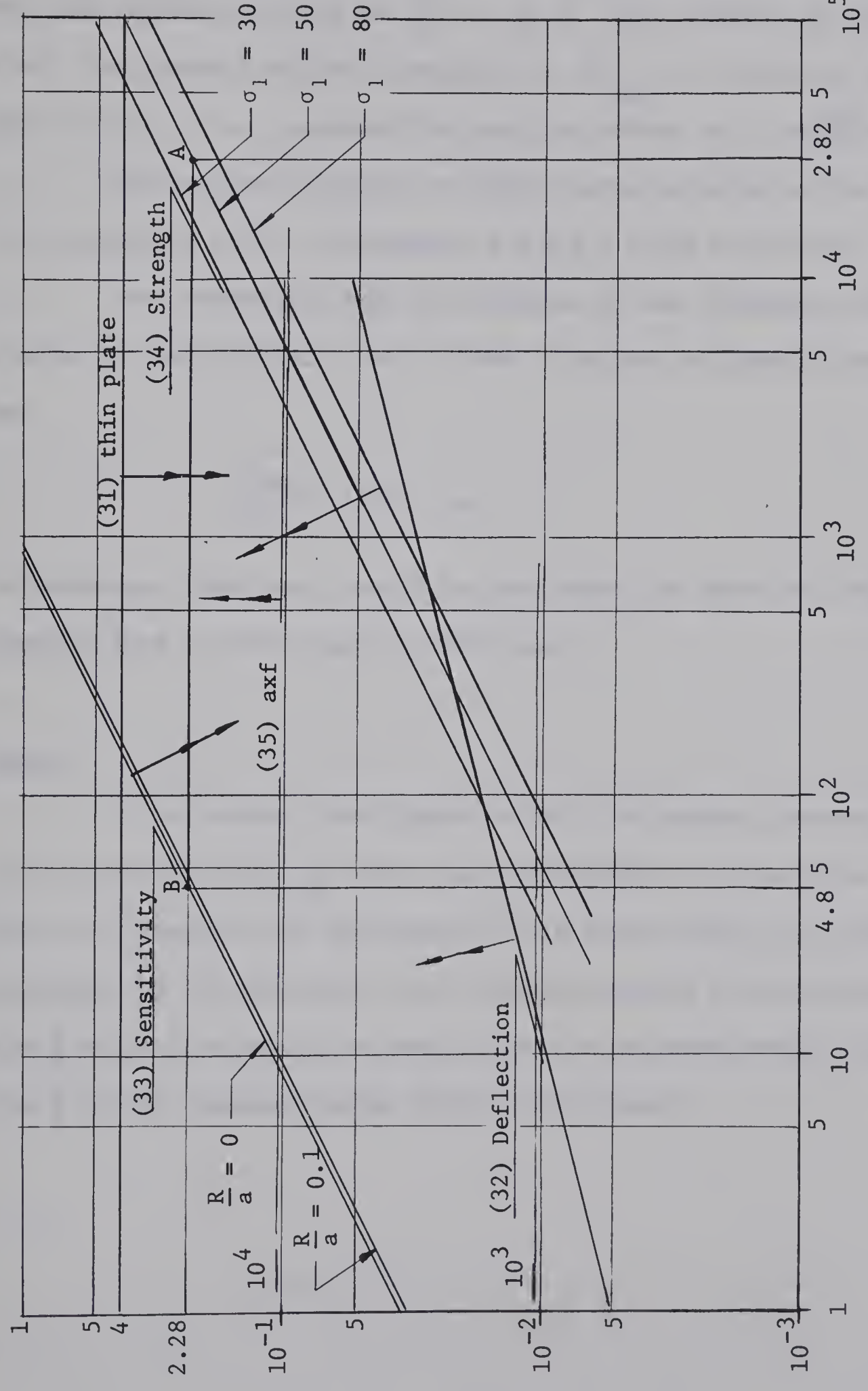

FIGURE 14. Design Chart for Diaphragm Type Load Transducer for $\frac{b}{a}$ = 0.1

σ_1 = 50,000 psi at A where $\frac{h}{a}$ = 0.228. The horizontal line through A intersects the sensitivity line for $\frac{R}{a}$ = 0 at B. The abscissa of point B is 48 psi, the lowest pressure measurable at $\bar{e}_{t_{min}}$ = 1 μ-in./in. So under the load of 50 lb., i.e., pressure 706 psi, the strain will be $\frac{706}{48}$ = 14.7 μ-in./in.

The optimum thickness to radius ratio is given by the ordinate of A or B, which is 0.228. Therefore, h = 1.5 x 0.228 = 0.342 in.

The fundamental mode of vibration of the diaphragm with $\frac{h}{a}$ = 0.228 is given by the relation a x f = 2000 from the horizontal lines marked a x f. Thus,

$$f = \frac{2000}{1.5} = 1333 \text{ cps} .$$

The diaphragm, therefore, should be used where the expected frequency of transient load is much less than 1333 cps.

Remarks

It is evident from Figure 14 that the maximum pressure for which a load transducer, with $\frac{b}{a}$ = 0.1, can be designed is of the order of 10^5 psi. Unless the dimension "b" and hence,"a" are large enough, the load that can be measured by the diaphragm type transducer cannot be very large for the ratio $\frac{b}{a}$ = 0.1 (for which the design chart 14 has been drawn). However, for other $\frac{b}{a}$ ratios, similar design charts can be drawn.

CHAPTER VII

EXPERIMENT ON A LOAD TRANSDUCER AND RESULTS

Experiments were conducted on a transducer designed according to Figure 14 and the example discussed in Chapter VI. The load was applied uniformly by means of a load distributor as shown in Figure 15. Three types of strain gauges were used in these experiments to compare their performances.

In the first experiment a B.L.H. diaphragm gauge, type FASE-25-12S6 having a radius of $\frac{1}{8}$ in., was placed at the center of the bottom surface of the diaphragm. A gauge factor of 2.1 was set on the selective dial of the indicator. The strain readings for different loads are shown in Figure 16.

The second experiment was conducted with two "special transducer quality" B.L.H. foil gauges, type FAE-06S-12S6 having a gauge length of $\frac{1}{16}$ in., placed on the bottom surface, one at the center and the other near the edge. These two gauges were connected in the two adjacent arms of the Wheatstone bridge circuit of the indicator. The combined strain output from the indicator has been plotted against the applied loads in Figure 17.

In the third experiment Budd strain gauges, type C6-111 having a gauge length of $\frac{1}{16}$ in., were used in place of B.L.H. gauges. The experiment was conducted in the same manner as the second one. The combined strain outputs for corresponding applied loads are shown in Figure 18.

Remarks

The spiral gauge exhibited good linearity in the first experiment, as shown in Figure 16. The maximum deviation of experimental points was 1.6 per cent of the full scale. No comparison with the theoretical strain

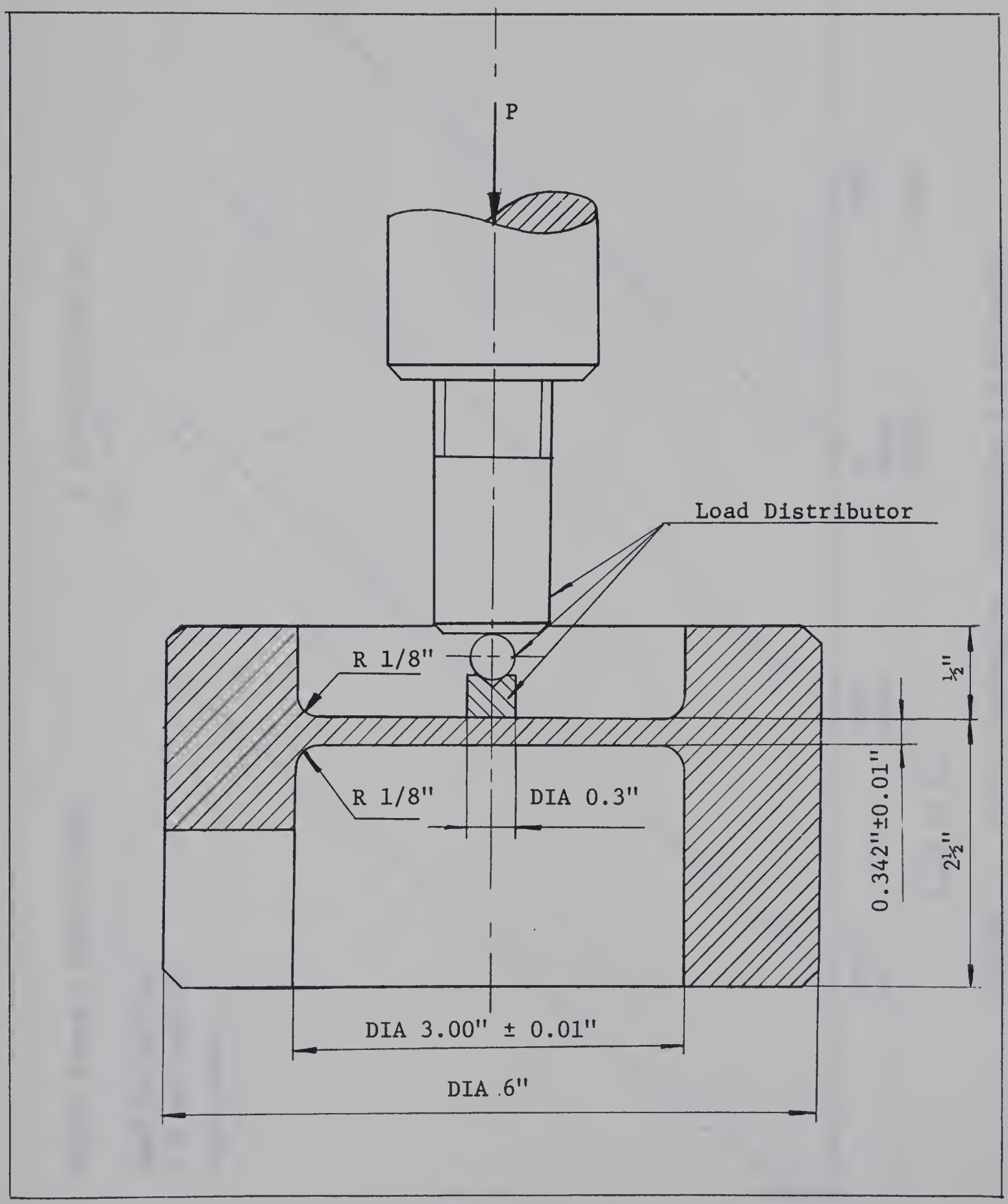

FIGURE 15. ARRANGEMENT FOR EXPERIMENT WITH DIAPHRAGM

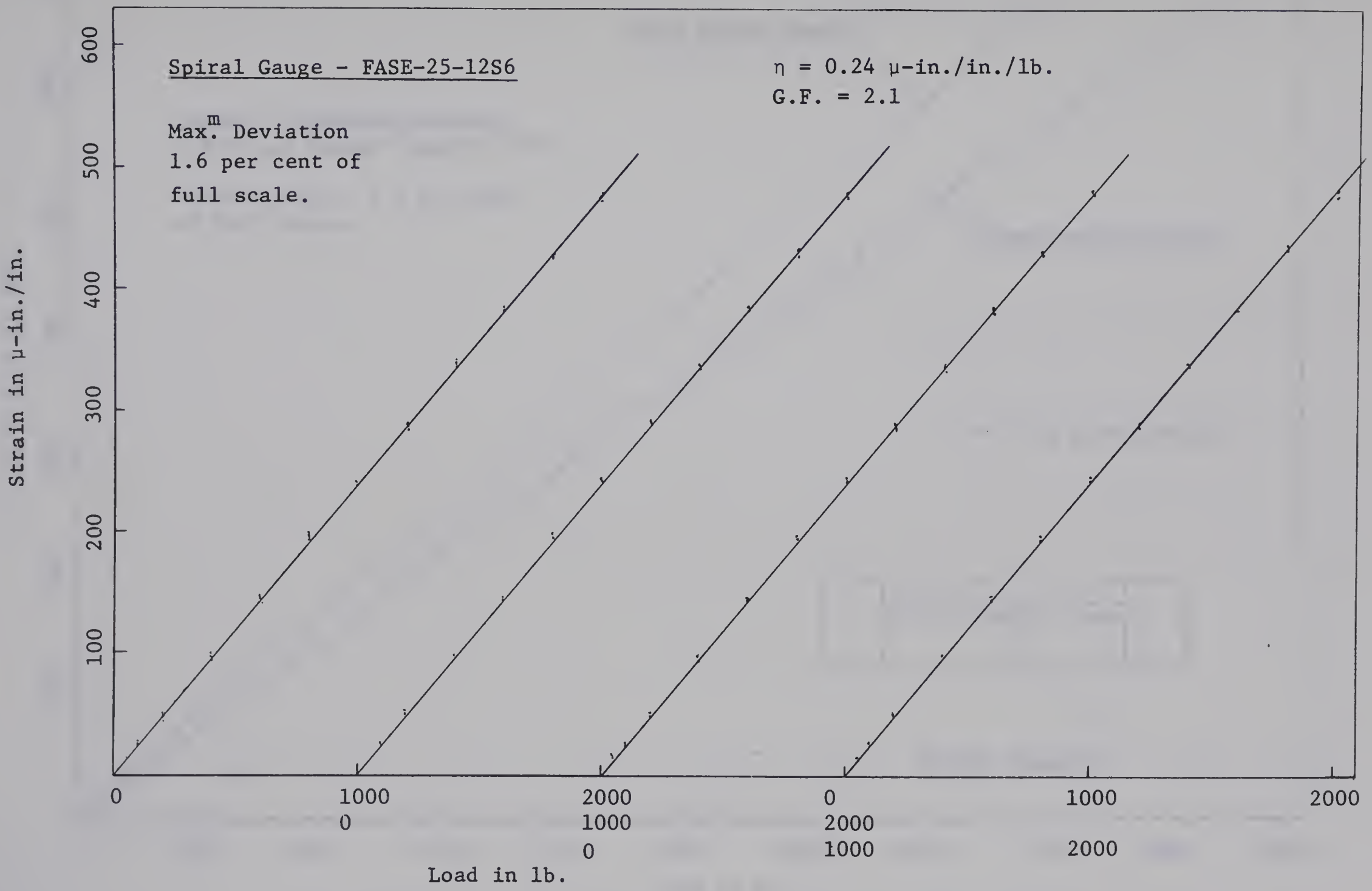

FIGURE 16. Strain Reading vs. Load Curve for Diaphragm

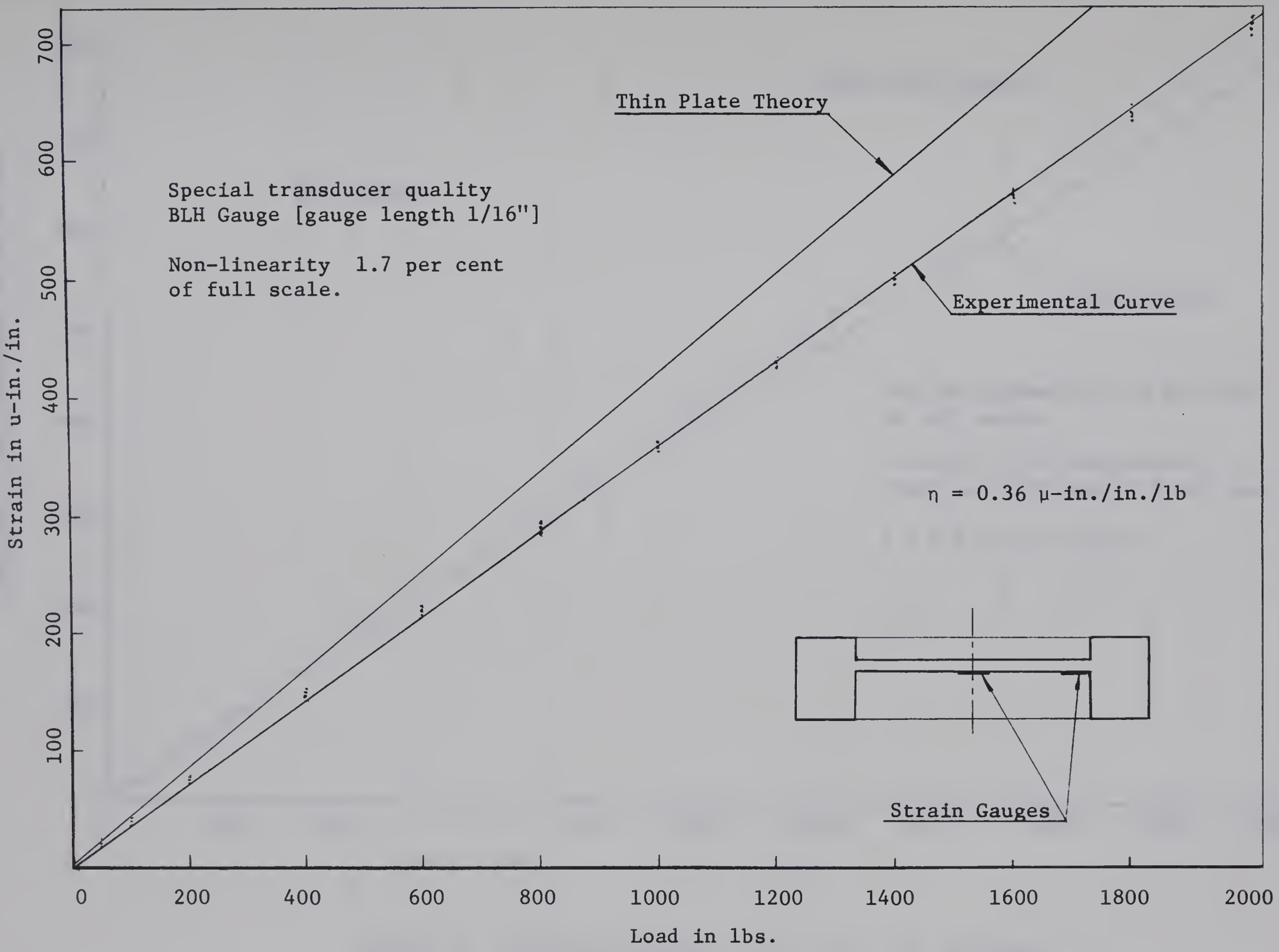

FIGURE 17. Combined Strain vs. Load Curve for Diaphragm

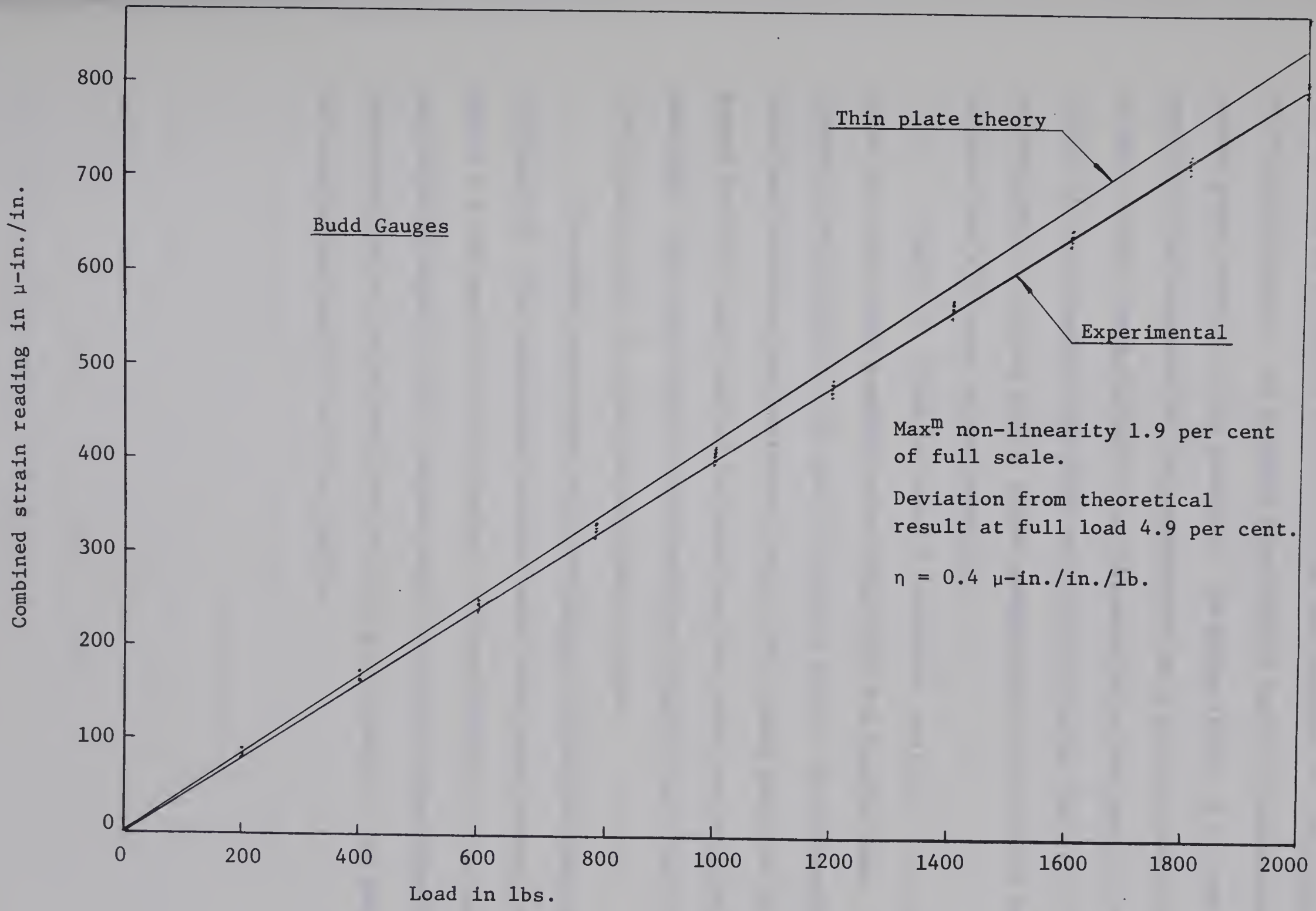

FIGURE 18. Combined Strain vs. Load Curve for Diaphragm

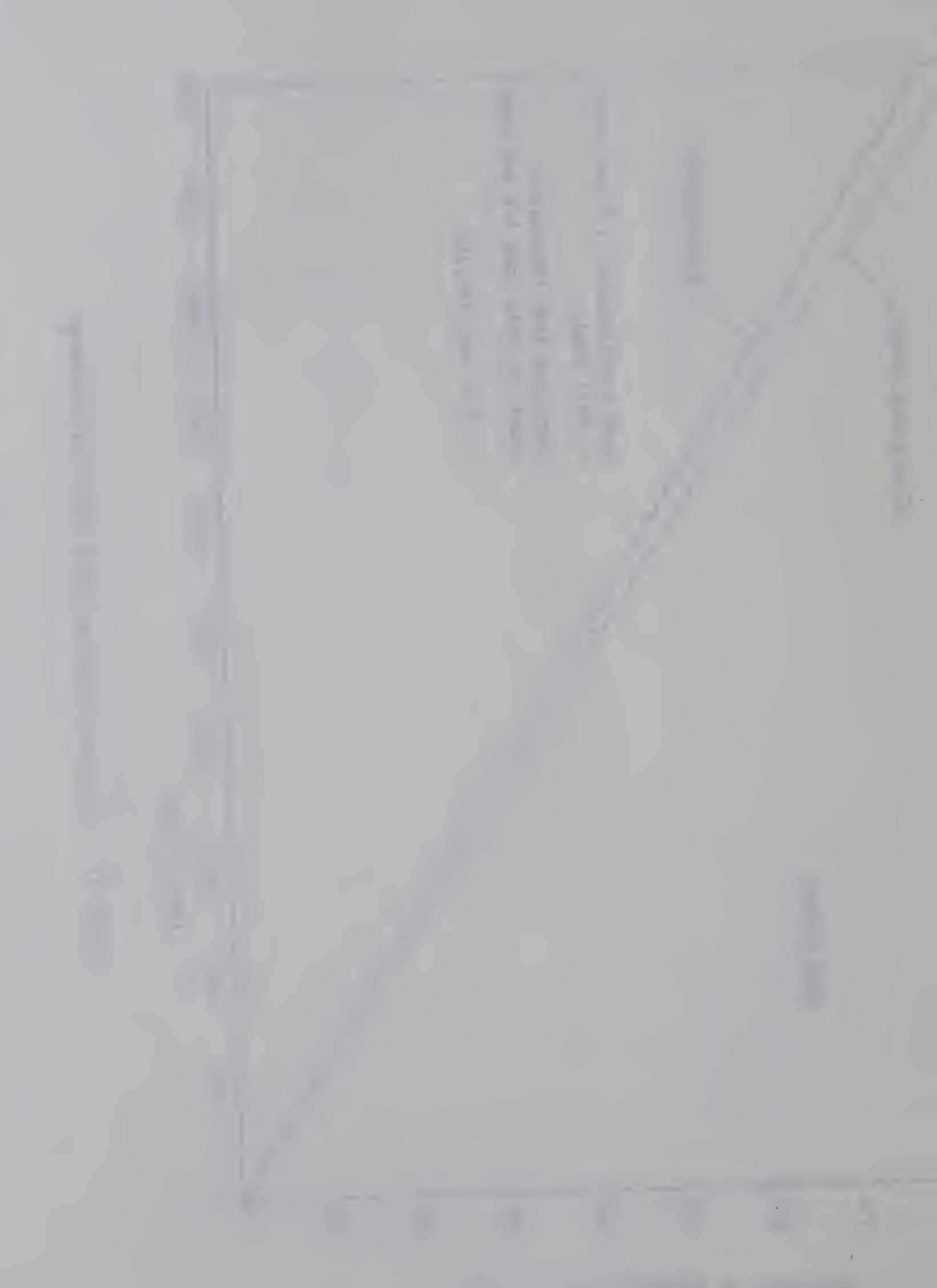

value could be attempted because of the arbitrariness of the gauge factor of the spiral gauge. An accurate gauge factor cannot be determined for the spiral gauge because of its geometry. The gauge factor, 2.1, used in the experiment was suggested by the manufacturer in a private communication. It is, in fact, the gauge factor for the material of the gauge. The sensitivity of the transducer was found to be 0.24 μ-in./in. per lb. A change in the gauge factor may give a higher sensitivity, but it is not known what effects this will have on the linearity.

Figure 17, drawn for special transducer quality B.L.H. gauges, shows that the strain readings were linear with the applied load. The linearity was within 1.7 per cent of the full scale. But the experimental curve was far below the theoretical curve. The reason might be that the gauges were not positioned in the locations for which the calculation had been made. The sensitivity of the transducer assembly was found to be 0.36 μ-in./in. per lb. from the experimental curve.

The third experiment with Budd gauges yielded the results shown in Figure 18. The experimental strains were linear with the applied loads within 1.9 per cent of the full scale. The experimental strain (combined two radial strains) at full load was only 4.9 per cent lower than the theoretical value (calculated from the thin plate theory). The sensitivity for this set-up was 0.40 μ-in./in. per lb.

CHAPTER VIII

CONCLUSION (PART B)

The design chart, Figure 14, constructed by following Werner's method, is a convenient aid for designing load transducers. Similar design charts can be constructed for different materials and different $\frac{b}{a}$ ratios, using equations (31) to (35). The experimental results agree with the thin plate theory to a very close degree, even for $\frac{h}{a} = 0.228$, as shown in Figure 18.

From the experimental results, it may be concluded that all the three types of gauges--B.L.H. diaphragm gauge, Budd foil gauge and B.L.H. special transducer quality gauge--show good reproducibility of the results for different loading cycles. Non-linearities of strain-load relationship, shown by these three types of gauges, are of the same order. The linearity of the said relationship can be evidently improved by taking extra precautions in fixing the strain gauges, sealing the gauges from moisture (which affects the performance of the gauges), using more accurate strain indicator and the associated circuitry. None of the disadvantages of the spiral gauge which have been referred to by Wenk--non-linearity of response, hysteresis and poor temperature compensation--was found in this particular investigation. This may be due to the fact that the design and the quality of the spiral gauges are much better today than those obtainable in the time of Wenk's publication (1951). The disadvantages that may be ascribed to spiral gauges are the comparatively higher cost and the indeterminate nature of their gauge factor. The latter makes the strain readings arbitrary and hence the theoretical average tangential strains cannot be verified from the spiral gauge readings.

The sensitivity of the transducer using Budd strain gauges for the same load range is higher than that obtained by using the other two types of gauges. It was not verified whether a transducer using a spiral gauge with a different setting of the gauge factor would give a higher sensitivity without impairing its linearity of response.

PART C

OTHER TYPES OF LOAD CELLS

CHAPTER IX

OTHER LOAD CELLS

9.1 Purpose

Two other load transducers commonly employed are the cylindrical and the fork types. The purpose of this chapter is to set up design procedures for these types following the same method used in the case of the diaphragm type. A comparison is made for these load transducers in relation to load range, sensitivity and frequency response for the same overall dimension of the transducer elements.

9.2 Cylindrical Type Load Transducer

If a cylindrical body, shown in Figure 19, be compressed, the strains at a point on the surface of the cylinder are given by the following expressions:

$$\text{Axial strain} \quad e_x = -\frac{4P}{\pi d^2 E}$$

$$\text{Circumferential or radial strain} \quad e_r = \frac{4\mu P}{\pi d^2 E}$$

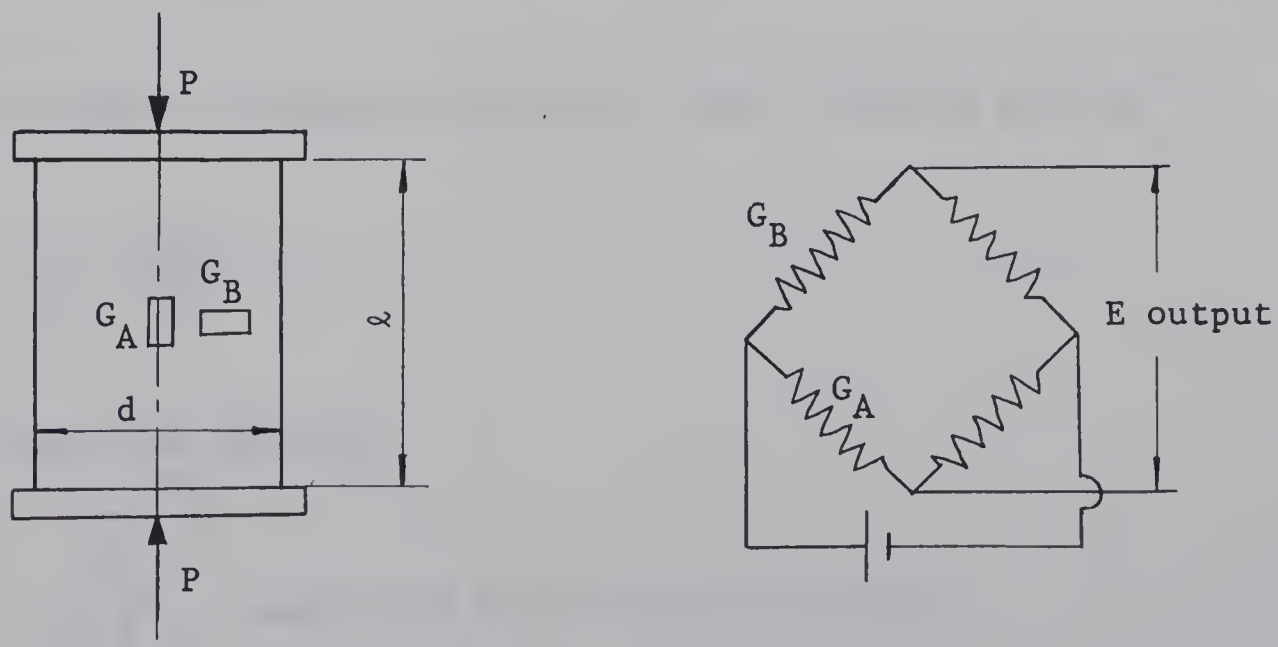

FIGURE 19. Cylindrical element and the Wheatstone Bridge Circuit

If the two strain gauges G_A and G_B are connected in the two adjacent arms of a Wheatstone bridge circuit as shown in Figure 19, the combined strain reading from the indicator will be given by

$$e_c = e_r - e_x = \frac{4P}{\pi d^2 E} (1 + \mu) . \qquad \ldots (36)$$

In accordance with the design procedures of Chapter VI, the following conditional equations relating the cylinder diameter d with its length may be derived:

i) For adequate sensitivity, it is required that

$$\frac{e_c}{P} \geqslant \frac{e_{c\ min}}{P_{min}}$$

where $e_{c\ min}$ is the minimum desired strain reading at the lowest load P_{min}. Substitution of expression (36) for e_c in this inequality leads to the following conditional relation,

$$d^2 \leqslant \frac{4\ P_{min}}{\pi e_{c\ min} E} (1 + \mu) \qquad \ldots (37)$$

ii) If the ends are assumed pinned, the lowest buckling load is

$$P_{cr} = \frac{\pi^2 EI}{\ell^2} .$$

Working load P must then satisfy

$$P \leqslant \frac{P_{cr}}{5}$$ where five is the factor of safety.

Thus,

$$d^4 \geqslant \frac{320\ \ell^2}{\pi^3\ E}\ P\ . \qquad \ldots (38)$$

iii) The load P must satisfy the following condition in order to avoid failure in compression:

$$P \leqslant \frac{\pi}{4}\ d^2\ \frac{\sigma_1}{2}\ .$$

where σ_1 is the allowable compressive stress of the material and two is an arbitrary factor of safety. This results in

$$d^2 \geqslant \frac{8P}{\pi\sigma_1}\ . \qquad \ldots (39)$$

iv) For uniform distribution of stress at the middle of the cylinder length, where the strain gauges are mounted, it is suggested that

$$d \leqslant \frac{\ell}{3}\ . \qquad \ldots (40)$$

v) The fundamental frequency of the cylinder is given by Timoshenko[14] as

$$f = \frac{1}{2\ell}\sqrt{\frac{Eg}{\gamma}}$$

$$= \frac{0.952 \times 10^5}{\ell}\ \text{cps.} \qquad \ldots (41)$$

The graphs d vs. P are plotted in Figure 20, using equations (37) to (40) to obtain a design chart for a cylindrical transducer. The area indicated by arrows in Figure 20 represents the zone of optimum functioning of the transducer. The abscissae of the intersection points of a horizontal line corresponding to a particular "d" with the sensitivity line on the left and with the buckling line or the strength line on the right, denote the load range for which the transducer performs satisfactorily. The use of Figure 20 in designing a transducer is explained by the following example.

Example Using Figure 20

A cylindrical transducer is to be designed for a load range of 2000 lb to 40,000 lb with a minimum strain reading of 20 μ-in./in. at the lowest load.

Let ℓ be equal to 4 in. and σ_1 be 60,000 psi for the material. A vertical line is drawn on the load axis at 40,000 lb. The line intersects the strength line σ_1 = 60,000 psi at A. The ordinate of A is 1.3 in. denoting the designed diameter of the cylindrical transducer. The horizontal line through A intersects the sensitivity line, which is drawn for $e_{c\ min}$ = 1.0 μ-in./in. at a load of 24 lb. This means that even at 24 x 20, i.e., 480 lb, this transducer will give a minimum strain reading of 20 μ-in./in.

From equation (41), the natural frequency of the bar is $\frac{0.952 \times 10^5}{4}$ cps., that is, 0.238×10^5 cps. The combined strain reading e_c will be 1330 μ-in./in. under the load of 40,000 lb from equation (36).

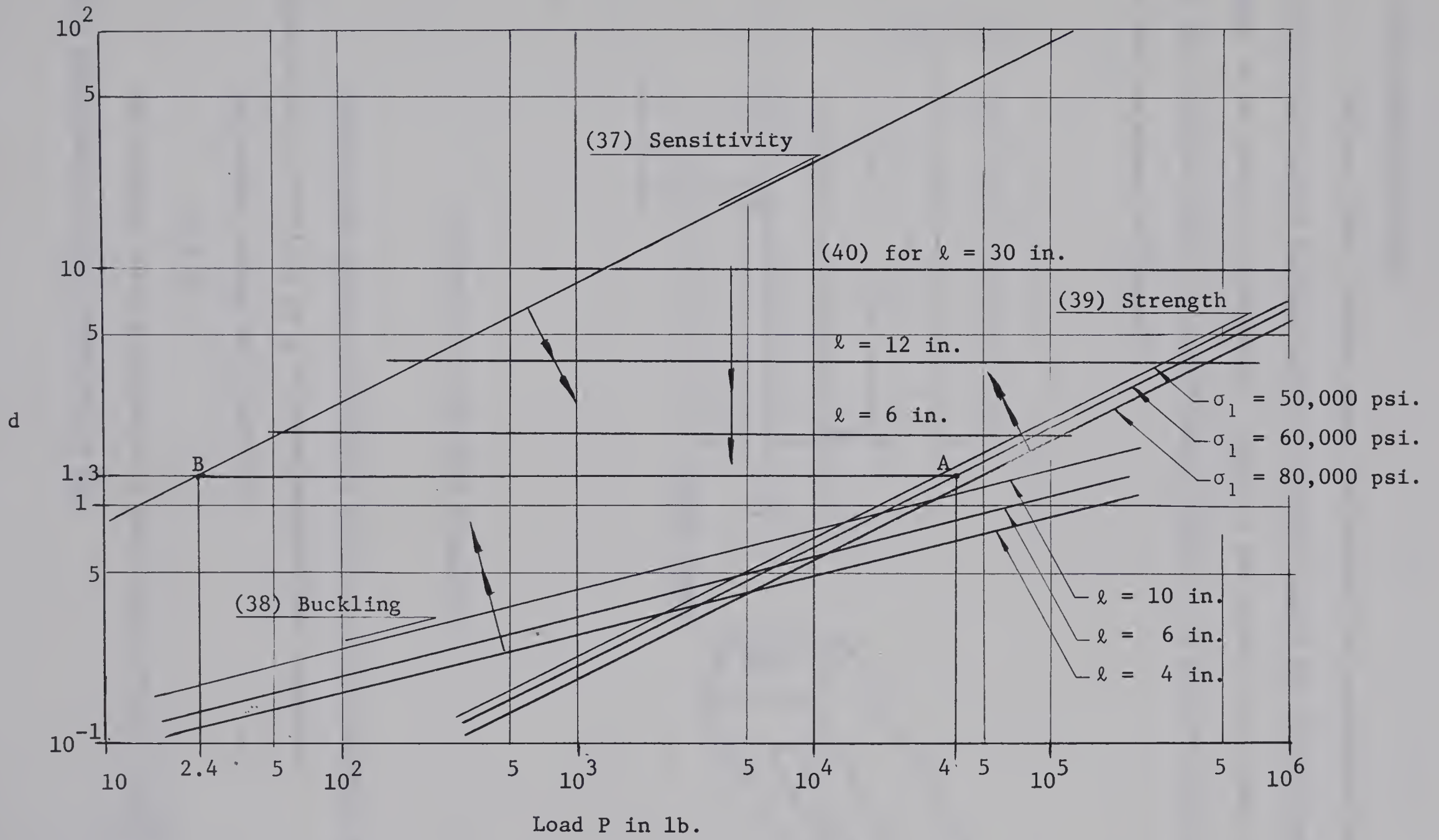

FIGURE 20. Design Chart for a Cylindrical Transducer

9.3 Fork Type Transducer

The fact that a strain gauge can convert the mechanical strain to electrical signals through proper circuitry allows any form of mechanical element to be used in a transducer, provided the element can convert the load into strains which are significantly large. One form of such an element is a fork as shown in Figure 21.

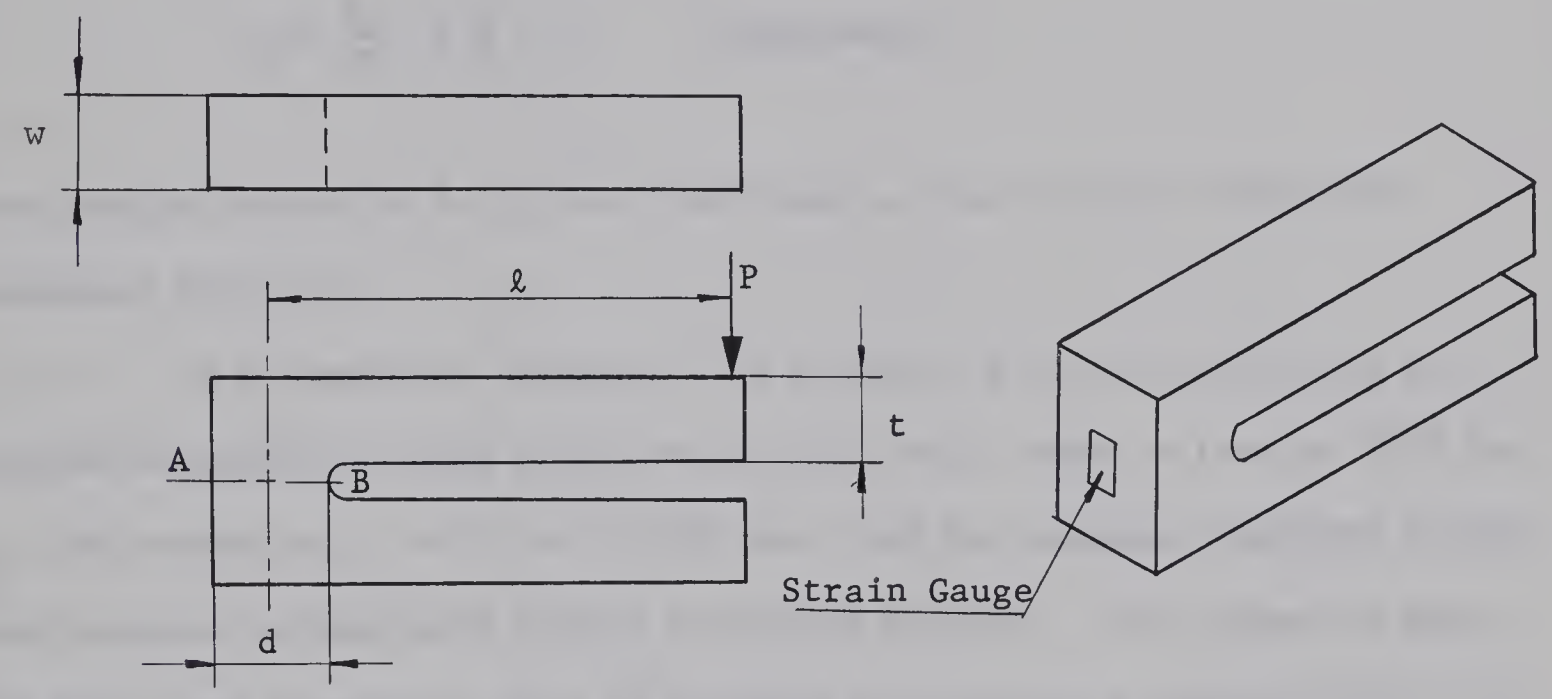

FIGURE 21. Fork Type Transducer

Simple beam theory is used here for theoretical analysis of this problem without resorting to a rigorous mathematical approach.

The moment across AB is given by

$$M = P\ell \ .$$

The maximum bending stress at A and B due to M will be $\frac{6P\ell}{wd^2}$. The direct compressive stress across AB is $\frac{P}{wd}$.

Therefore, resultant stresses at A and B are given by the following expressions:

$$\sigma_A = \frac{P}{wd}\left(6\frac{\ell}{d} - 1\right) \qquad \text{tensile,} \qquad \ldots (42)$$

and

$$\sigma_B = \frac{P}{wd}\left(6\frac{\ell}{d} + 1\right) \qquad \text{compressive.}$$

The tensile stress at A, σ_A, will be taken as the critical stress for designing the fork.

As a numerical example, if ℓ = 6 in., d = 1 in. and w = 1 in. and the material is steel with E = 29 x 10^6 psi., under a load of 3000 lb, σ_A, the stress at A, will be 105,000 psi. and for commonly employed steels this value of stress will exceed the yield strength. This suggests that the fork type transducer will be suitable for measuring comparatively low loads, unless a different material or larger dimensions are used.

To decrease the number of parameters, load per unit width will be used for design calculations, that is, $Q = \frac{P}{w}$ will be used in place of P.

The strain at A is then expressed by the following equation,

$$e = \frac{Q}{dE}\left(6\frac{\ell}{d} - 1\right) \qquad \ldots (43)$$

Design Procedure

The conditional inequalities for a dimensional parameter with other parameters are set up following the same method, as was followed in Chapter VI and Section 9.2.

a) For adequate sensitivity, i.e., to assure a minimum strain reading e_{min} at the minimum load Q_{min}, the following inequality results from the expression (43) for strain,

$$\frac{\ell}{d} \geqslant \frac{1}{6}\left(\frac{e_{min}}{Q_{min}}\, dE + 1\right) . \qquad \ldots (44)$$

b) From the point of view of the strength of the material, if the maximum allowable stress be σ_1 and a factor of safety two is assumed, an inequality of the following form is obtained:

$$\frac{\ell}{d} \leqslant \frac{1}{6}\left(\frac{\sigma_1\, d}{2\, Q_{max}} + 1\right) . \qquad \ldots (45)$$

This follows from the inequality $\sigma_A \leqslant \frac{\sigma_1}{2}$, where σ_A is substituted from equation (42).

c) The deflection at the load application point should not be more than some specified value $\delta_{max} = 0.02\ell$, so that the simple beam theory may be applied. Assuming the top side of the beam as a cantilevered beam, it follows:

$$\frac{1}{3}\frac{Q\ell^3}{EI} \leqslant \delta_{max} = 0.02\ell .$$

Hence, $$\frac{4\, Q_{max}}{E}\left(\frac{\ell}{t}\right)^3 \leqslant 0.02\ell . \qquad \ldots (46)$$

d) The fundamental frequency, f, of a bar fixed at one end and free at the other is given by Timoshenko[15] as

$$f = \frac{a}{2\pi} \left(\frac{1.875}{\ell}\right)^2 , \quad \text{where} \quad a = \sqrt{\frac{EIg}{A\gamma}}$$

$$= 3.075 \times 10^4 \times \frac{t}{\ell^2} \qquad \ldots (47)$$

In practice, the natural frequency of the bar is chosen much higher than the expected frequency of the applied transient load, f_w. This gives the following condition,

$$\frac{\ell}{t} \leq \frac{3.075 \times 10^4}{\ell \times f_w} \quad . \qquad \ldots (48)$$

The equations (44) to (46) and (48) are generally plotted to obtain a design chart for a fork type transducer. To reduce the number of parameters it is assumed that d = t. Depending on circumstances, a fixed d may be chosen and a set of graphs corresponding to expressions (44) to (46) and (48) may be drawn for a suitable design of $\frac{\ell}{d}$ ratio. Conversely, a fixed ℓ may be chosen and a set of graphs for $\frac{\ell}{d}$ vs. Q may be drawn to design optimum d.

Figure 22 has been drawn taking "d" as constant and equal to $\frac{3}{4}$ in. In plotting the equations (44) and (45) only the dominating terms inside the parentheses, i.e., $\frac{e_{min}}{Q_{min}}\, dE$ and $\frac{\sigma_1 d}{2\, Q_{max}}$, which are normally much greater than one, have been taken into account.

The area indicated by arrows in Figure 22 shows the zone of satisfactory design of the transducer. The use of this Figure for design purposes is explained by the following example.

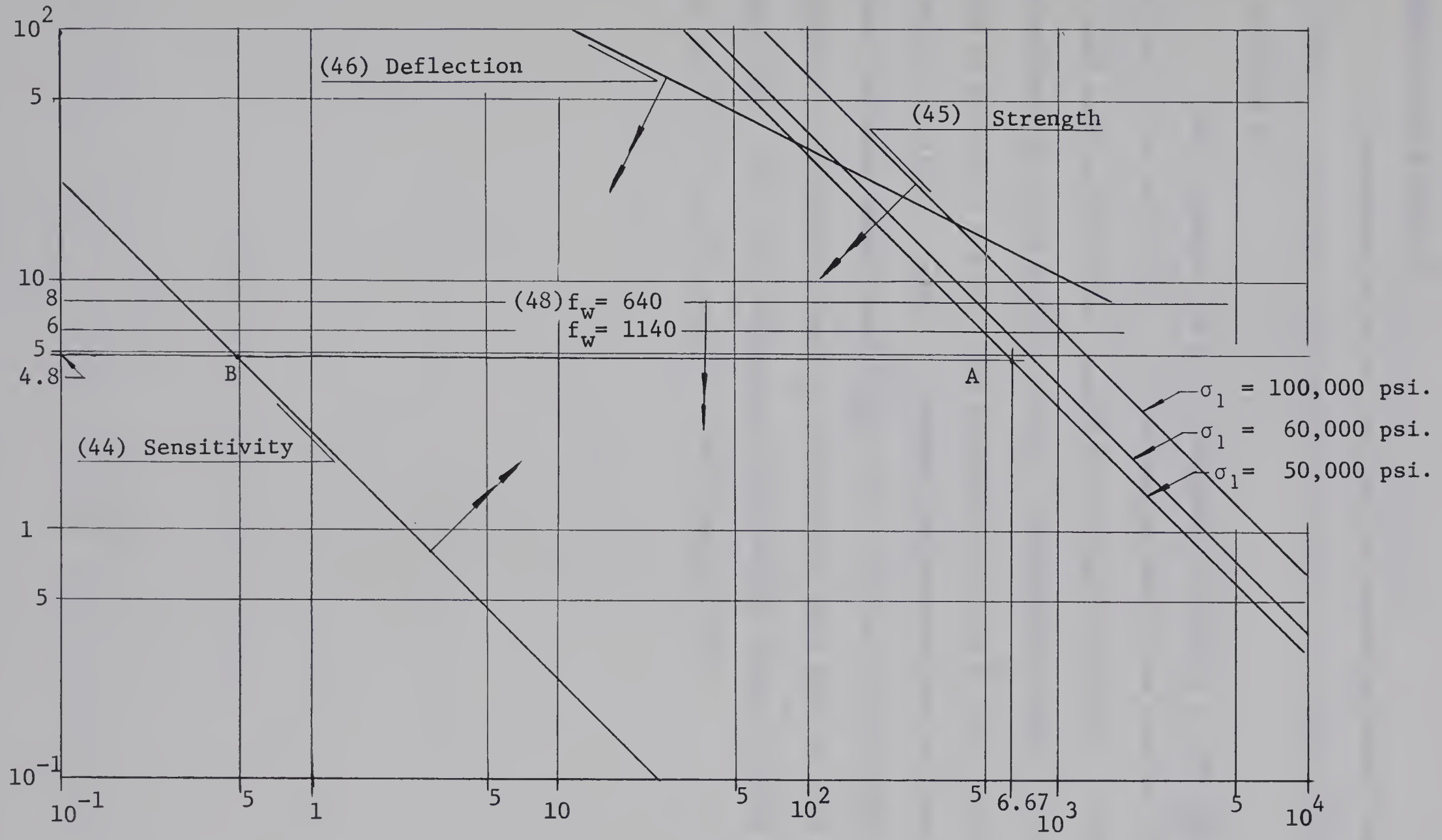

FIGURE 22. Design Chart for Fork Type Transducer for d = $\frac{3}{4}$ in.

Example Using Figure 22

A transducer is to be designed for measuring loads from 5 to 500 lb. The width w, thickness t and depth at the neck d are equal to $\frac{3}{4}$ in. and σ_1 = 50,000 psi.

The transducer is to be designed to measure Q from $\frac{5}{3/4}$ to $\frac{500}{3/4}$ lb/in., that is, 6.7 to 667 lb/in. In the design chart, the vertical line drawn on the load axis at 667 lb/in. meets the strength line for σ_1 = 50,000 psi at A. The ordinate $\frac{\ell}{d}$ of the point A is 4.8. The designed length "ℓ", therefore, is equal to $\frac{3}{4}$ x 4.8 = 3.6 in. The horizontal line at $\frac{\ell}{d}$ = 4.8 cuts the sensitivity line at 0.50 lb/in. load. To measure the minimum load of five pounds, the strain indicator should read $\frac{6.70}{0.50}$ = 13.4 μ-in./in. at the lowest limit. The frequency of fundamental mode of vibration of this fork is 1780 cps. from graphs (48). For this configuration the maximum tensile strain at A under a load of 500 lb is 852 μ-in./in. from equation (43).

CHAPTER X

EXPERIMENTS AND RESULTS

10.1 Cylindrical Type Transducer

An experiment was conducted on a cylindrical type transducer to verify the equations developed in Section 9.2. The specimen and the general arrangement is shown in Figure 23.

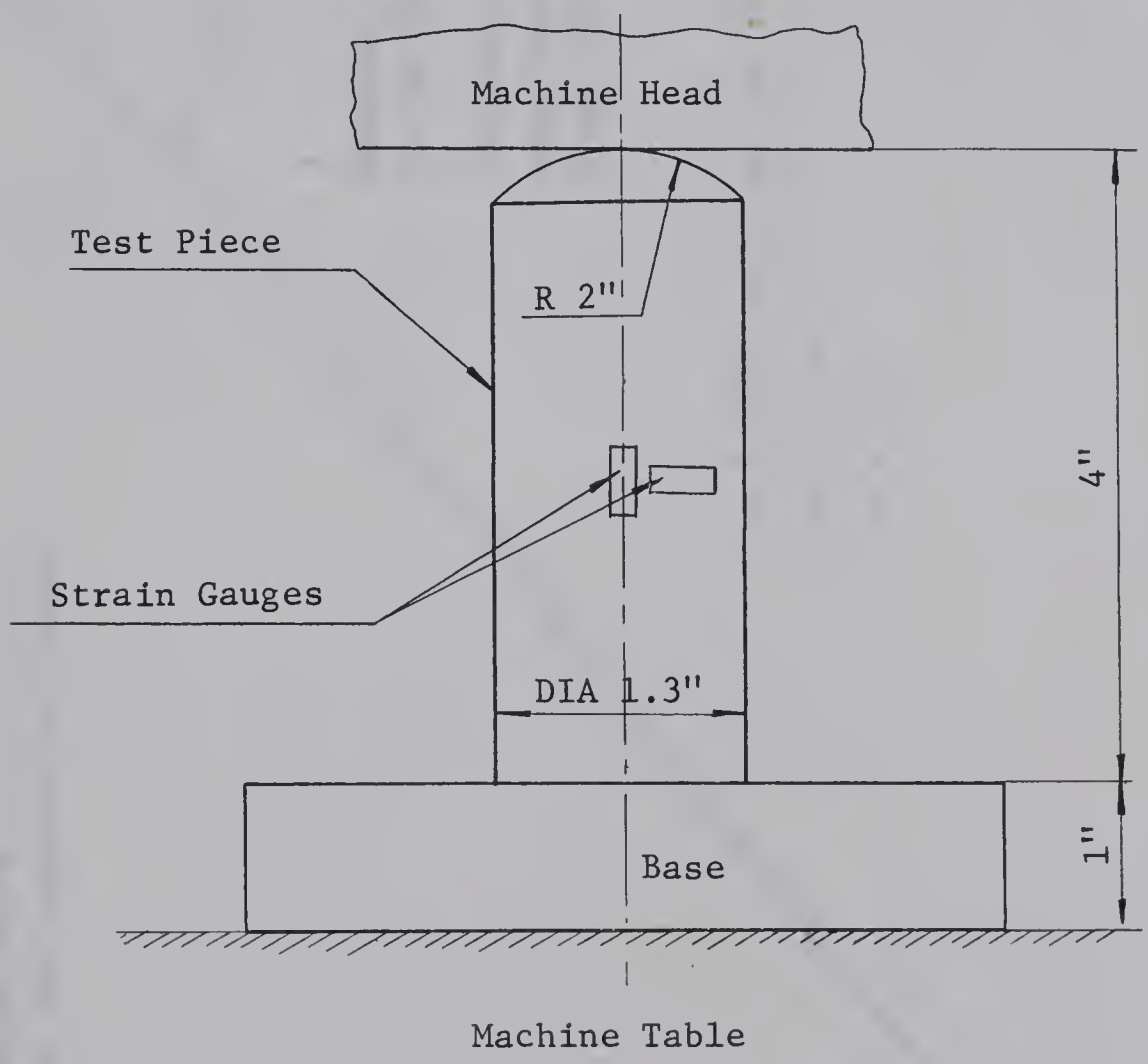

FIGURE 23. Cylindrical Transducer

Budd gauges, type C6-111 having a gauge length of $\frac{1}{16}$ in., were used. The combined strain output from the experiment has been plotted against the applied load in Figure 24.

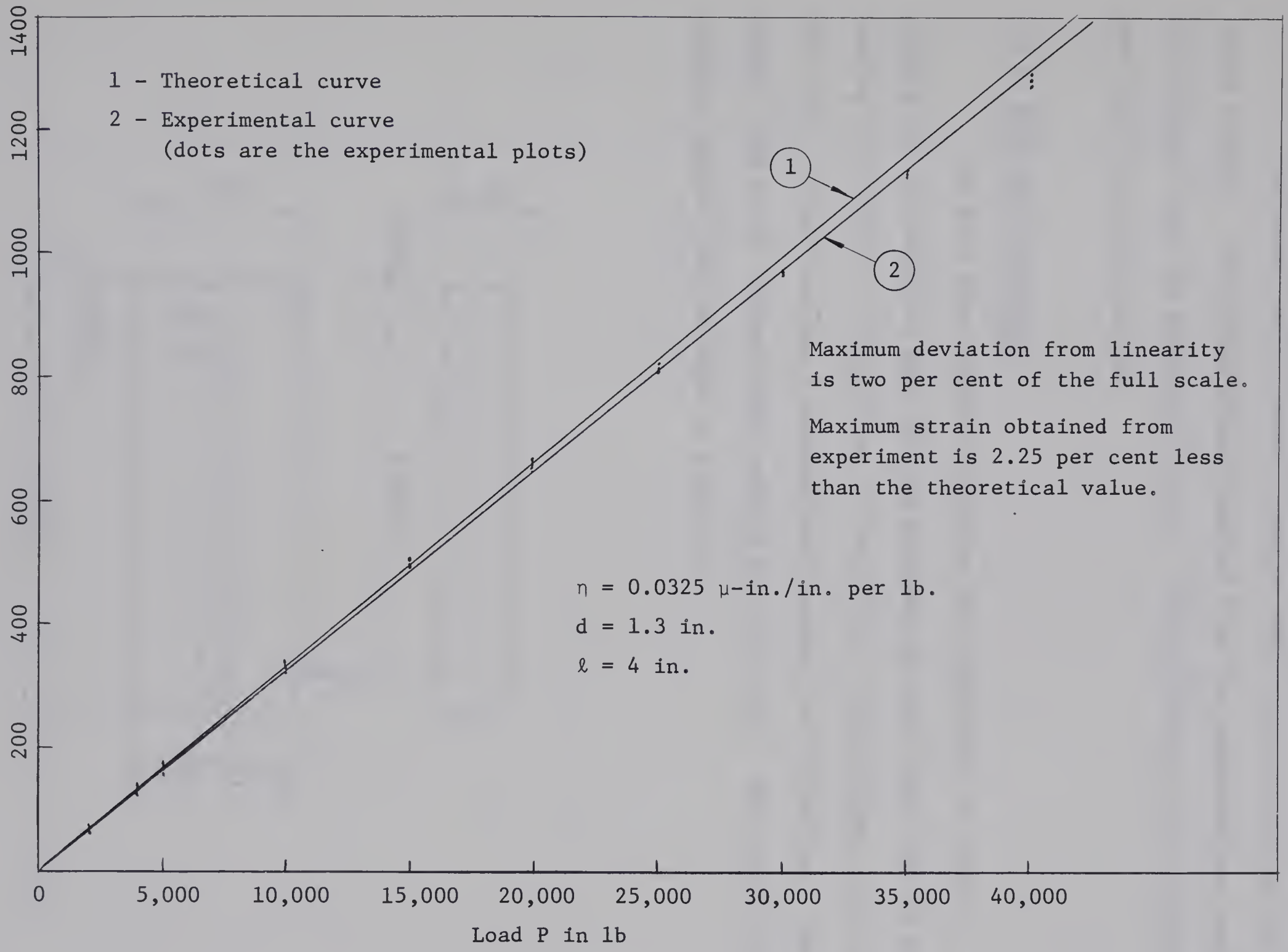

FIGURE 24. Combined Strain vs. Load Curve for Cylindrical Type Transducer

Remarks

The output strain showed linearity within two per cent of the full scale reading. The maximum strain obtained from the experiment was less by 2.2 per cent than the theoretical value. The sensitivity of the transducer was 0.0325 μ-in./in. per lb.

10.2 Fork Type Transducer

The fork type transducer used in this experiment is shown in Figure 25. The material used for the specimen was tool steel (USS T1 steel, having 0.12-0.21% C, 0.70-1.0% Mn, 0.40-0.65% Cr, 0.15-0.25% Mb, 0.03-0.08% Vn, etc.). This steel has a minimum yield strength of 100,000 psi. Budd gauge, type C6-121 (gauge length being $\frac{1}{8}$ in.), was used. The output strain against applied load is shown in Figure 26.

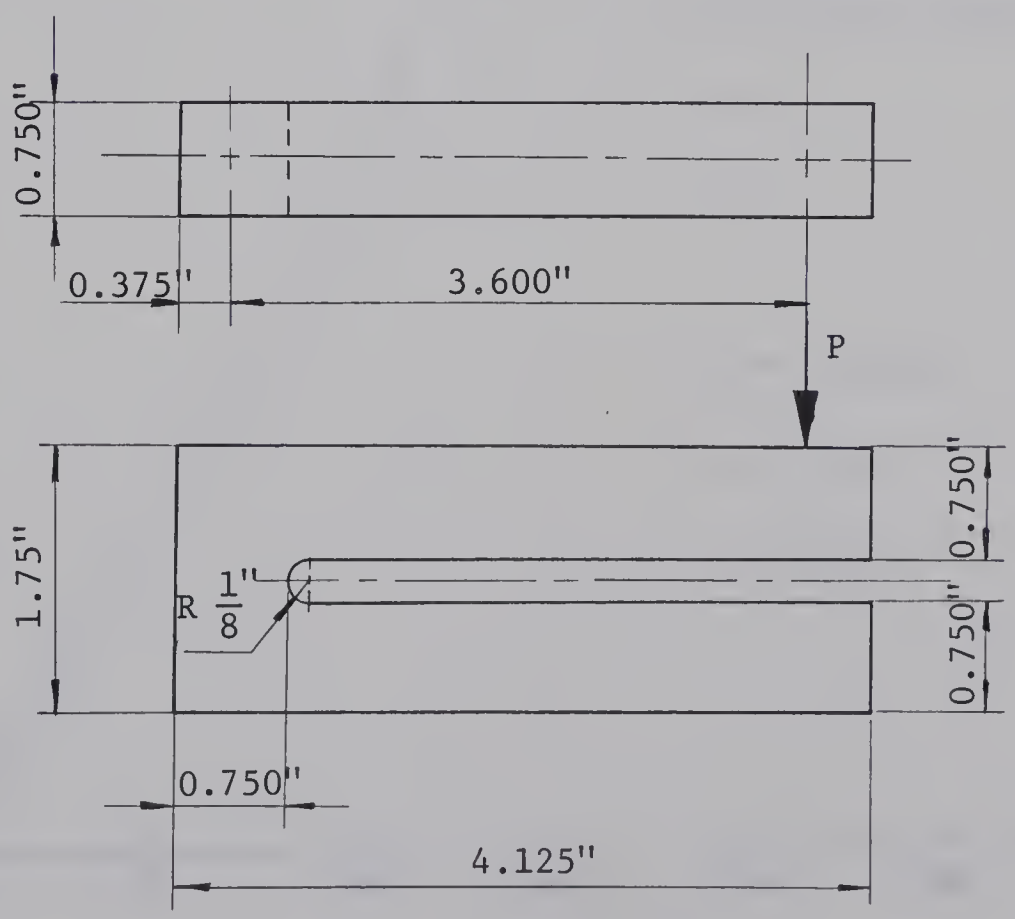

FIGURE 25. Fork Type Transducer

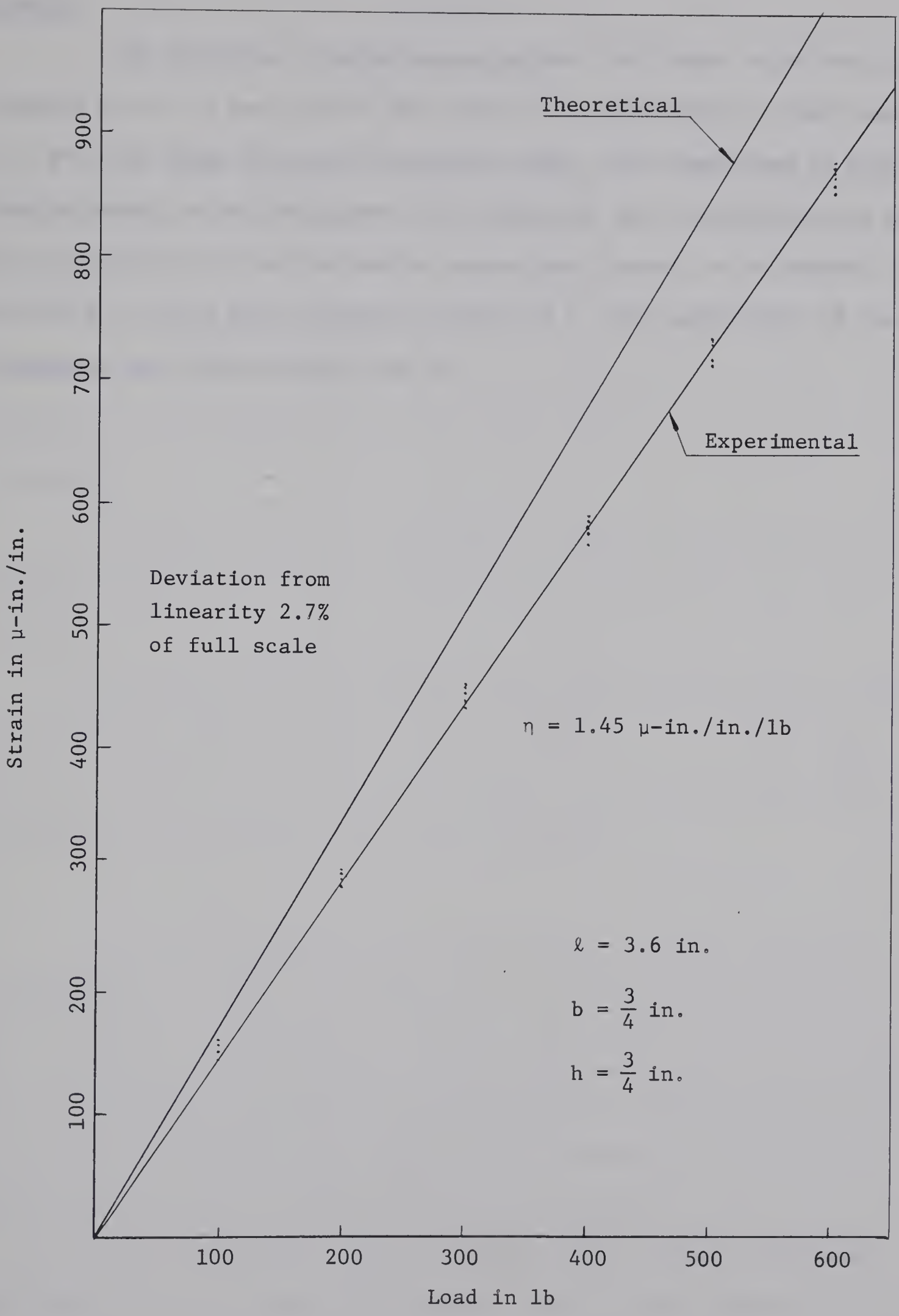

FIGURE 26. Strain vs. Load Curve for a Fork Type Transducer

Remarks

The deviation of experimental points from linear relationship was observed to be 2.7 per cent of full scale. The experimental strain was 15.3 per cent lower than the theoretical value. The reason may be that the bending moment calculated across AB in Figure 21 and its distribution along the cross-section do not follow the simple beam theory, as is assumed in Section 9.3, for a short length of lever arm ℓ. The sensitivity of the transducer was 1.45 μ-in./in. per lb.

CHAPTER XI

CONCLUSION (PART C)

On comparing the three types of elements of transducers investigated in this work for comparable overall sizes, the following observations can be made:

1) The cylindrical type transducer is suitable for higher loads, the diaphragm type for medium loads and the fork type for low loads. The magnitude of the loads will evidently depend upon the overall size of the transducer.

2) The cylindrical type transducer is comparatively insensitive, the diaphragm type is moderately sensitive, whereas the fork type is highly sensitive.

3) Because of geometry the frequency of natural vibration is high for cylindrical type, medium for diaphragm type and low for fork type. Where the expected frequency of the transient load is very high, it is preferable to use the cylindrical type of element.

For certain values of load there may be a choice between the cylindrical type and the diaphragm type or between the diaphragm type and the fork type. The final choice in such cases would depend on available space (the height of the available space may be a deciding criterion), the frequency of the load, ease in machining the element, and the protective enclosure that might be needed for the strain gauges.

One of the purposes of this thesis was to design a diaphragm type load cell for a maximum load range. From the above observations, a diaphragm type transducer can not be recommended for very high loads. But

the small height of the diaphragm cell may make its use justifiable in certain applications. The fork type transducer may also be made of small height. But its lower natural frequency of vibration and lower load carrying capacity may become disadvantageous. Finally, it is recommended that the thickness of the diaphragm cell be uniform, if the diaphragm is to be designed for a maximum load carrying capacity.

BIBLIOGRAPHY

1. Grey, Jerry, "Pressure Transducers," Product of Engineering, January 1954, pp. 174-179.
2. Bierman, H.R. and Jenkins, R., "A Hypodermic Pressure Manometer Utilising the Bonded Wire Resistance Strain Gage," The Review of Scientific Instruments, Vol. 22, 1951, p. 268.
3. Bierman, H.R., "A Device for Measuring Physiological Pressure Phenomena Using the Bonded Electrical Wire Resistance Strain Gauge," The Review of Scientific Instruments, V 19, 1948, p. 707.
4. Wenk, E., "A Diaphragm Type Gauge for Measuring Low Pressure in Fluids," Proceedings of the Society for Experimental Analysis, Vol. 8, No. 2, 1951, pp. 90-96.
5. Werner, F.D., "The Design of Diaphragms for Pressure Gauges Which Use the Bonded Wire Resistance Strain Gauge," Proceedings of the Society for Experimental Analysis, Vol. 11, No. 1, 1953, pp. 137-146.
6. Lee, C.E., "A Portable Electronic Scale for Weighing Vehicles in Motion," Highway Research Record, No. 127, Publication 1370, 1966.
7. Love, A.E.H., A Treatise on the Mathematical Theory of Elasticity, Dover Publications, 1944, pp. 465-487.
8. Timoshenko, S.P. and Goodier, J.N., Theory of Elasticity, McGraw-Hill Book Company, 1951, pp. 375-376.
9. Ibid., pp. 343-352.

10. Hoeland, Günter, "Ein Beitrag zur Berechnung örtlich dickerer Platten," Beton und Stahlbetonbau, Heft 3, March 1959, pp. 65-69.

11. Love, op. cit., p. 479.

12. Love, op. cit., pp. 473-474.

13. Morse, P.M., Vibration and Sound, New York, 2nd Edition, p. 210.

14. Timoshenko, S., Vibration Problems in Engineering, Van Nostrand, 1955, p. 300.

15. Ibid., p. 338.